



Universität
Rostock



Traditio et Innovatio



SOLENT
UNIVERSITY
SOUTHAMPTON



Zachodniopomorski
Uniwersytet
Techniczny
w Szczecinie



**BUREAU
VERITAS**

Numerical Analysis of Composite Propeller for the Validation of a Fluid Structure Interaction Tool

Submitted on 29 August 2020

by

REHMAN Wajiha | 5 Rue des Renards | 44072 Nantes | wajiharehman11@gmail.com

Student ID No.: 190611K

Supervisor:

Mr. Stephane PABOEUF

Bureau Veritas Marine & Offshore (Head of Composite Material Section- Expertise Department)

8 BD Albert Einstein

44300 Nantes

France



This Master Thesis has been prepared as part of the graduation of the Master in Marine Technology specialized in Hydrodynamics for Ocean Engineering from Centrale Nantes and the graduation of the double Master degree Liège University-Centrale Nantes in the EMship+ programme

CONTENTS

LIST OF FIGURES	3
LIST OF TABLES	4
DECLARATION OF AUTHORSHIP	6
ABSTRACT	7
1 INTRODUCTION	8
1.1 Propeller's Geometry	10
1.2 Propeller Performance Characteristics	13
1.3 Objectives	14
1.4 Organization of the Project	15
2 SCANTLING AND RECONSTRUCTION OF PROPELLER'S GEOMETRY	17
2.1 Design Guidelines for the Laminates	18
2.2 Blade's Scantling:	20
3 FSI ANALYSIS BY RANS-FEM COUPLING	23
3.1 Calculations Done by the RANSE Solver	26
3.2 Geometry Preparation	27
3.3 Calculations Done by the FEM Solver	28
4 FSI ANALYSIS BY BEM-FEM COUPLING	31
4.1 Calculations Done by the BEM Solver	32
5 ISOTROPIC BLADE CASE	36
5.1 Case 1: BEM-FEM One-Way Coupled FSI Analysis	36
5.2 Case 2: RANS-FEM One-Way Coupled FSI Analysis	37
5.3 Case 3: BEM-FEM Explicit Two-Way Coupled FSI Analysis with Com- PropApp	37
5.4 Case 4: RANS-FEM Implicit Two-Way Coupled FSI Analysis with STAR- CCM+	38

5.5	Comparison	38
5.5.1	<i>Input Comparison</i>	38
5.5.2	<i>Output Comparison</i>	41
6	COMPOSITE BLADE CASE	50
6.1	Case 1: BEM-FEM One-Way Coupled FSI Analysis	50
6.2	Case 2: RANS-FEM One-Way Coupled FSI Analysis	50
6.3	Case 3: BEM-FEM One-Way Coupled FSI Analysis with ComPropApp .	51
6.4	Case 4: RANS-FEM Explicit Two-Way Coupled FSI Analysis with STAR- CCM+ and FEMAP	51
6.5	Comparison	52
6.5.1	<i>Input Comparison</i>	53
6.5.2	<i>Output Comparison</i>	54
7	CONCLUSION	61
	ACKNOWLEDGEMENTS	63
	REFERENCES	64
	APPENDIX 1	67

LIST OF FIGURES

1	Composite propellers	9
2	Propeller's geometry parameters	11
3	Demonstration of the helix line	11
4	Expanded view of the propeller's blade	12
5	Propeller's blade pitch	12
6	Hydrofoil geometry	13
7	FabHeli Propeller	14
8	Project organization	16
9	Laminates stacking sequences	17
10	Laminates stacking sequences	18
11	Ply-drop-off in laminate of varying thickness	19
12	Division of the blade into nine zones	21
13	Sequence of the laminates	22
14	Solution based classification of FSI	23
15	Two approaches for FSI analysis	23
16	Flow charts of one-way and two-way couplings	25
17	Propeller in fluid domain	28
18	Mesh generated by FEM solver	29
19	User interface of ComPropApp	31
20	Process flow chart of BEM-FEM coupling	32
21	General notation for Green's theorem application	33
22	Panel discretization of the propeller	35
23	Blade and wake discretization in Provise	35
24	Analysis performed for the isotropic blade case	36
25	Mesh used in case 1	39
26	Mesh used in case 2	40
27	Mesh used in case 3 (ComPropApp)	40
28	Mesh used in case 4 (STAR-CCM+)	41
29	Results obtained in case 1	42
30	Results obtained in case 2	42
31	Maximum displacement for case 3 (1.70 mm)	43

32	Results obtained in case 4	43
33	Comparison of the pressure side pressure	46
34	Comparison of the suction side pressure	46
35	Pressure difference at the middle of the blade	47
36	Pressure difference at the tip of the blade	47
37	Analysis performed for the composite blade case	50
38	Convergence graph of blade displacement	52
39	FEM mesh used for composite blade	53
40	Results obtained in case 1	54
41	Results obtained in case 2	55
42	Maximum displacement for case 3 (13.6 mm)	56
43	Results obtained in case 4	56
44	Imported vs. mapped displacement field	59
45	Actual vs. mapped pressure field	59
46	Results obtained in benchmark study	67

LIST OF TABLES

1	Characteristics of FabHeli	15
2	Properties of individual layers	21
3	Properties of the laminates used in propeller's scantling	22
4	Defined parameters in STAR-CCM+	28
5	FEM mesh convergence study	29
6	Material Properties	36
7	Summary of all the isotropic blade cases	38
8	Isotropic blade case: Mesh comparison	41
9	Isotropic blade case: Output comparison with complete FSI in ComPropApp	44
10	Comparison of the moments at blade root	45
11	Comparison of computation time for BEM and RANS FSI Analysis	49
12	Summary of all the cases	52
13	Composite blade case: Mesh comparison	53
14	Composite blade case: Output comparison with FSI in ComPropApp	57
15	Relative difference of imported and mapped Pressure and displacement fields	58

16	Comparison of computation time for BEM and RANS FSI Analysis . . .	60
17	Comparison of Hexahedral mesh and Tetrahedral mesh	68

DECLARATION OF AUTHORSHIP

I declare that this thesis and the work presented in it are my own and have been generated by me as the result of my own original research.

Where I have consulted the published work of others, this is always clearly attributed.

Where I have quoted from the work of others, the source is always given. With the exception of such quotations, this thesis is entirely my own work.

I have acknowledged all main sources of help.

Where the thesis is based on work done by myself jointly with others, I have made clear exactly what was done by others and what I have contributed myself.

This thesis contains no material that has been submitted previously, in whole or in part, for the award of any other academic degree or diploma.

I cede copyright of the thesis in favour of the Ecole Centrale de Nantes (ECN), France.

Date: 29/08/2020

Signature:

A handwritten signature in black ink, appearing to read 'Wajih', written over a horizontal line.

ABSTRACT

*Composite propellers are the potential alternative to conventional propellers because of their superior properties such as high specific stiffness and strength ratios. The industry is becoming aware of the advantages of composite propellers and an increasing trend towards it is noticed. Unfortunately, there is a lack of proper design assessment tools for the certification of composite propellers. Therefore, it is essential to develop and validate the tools to evaluate the design of the composite propellers. This report is about the validation of a design assessment tool known as **ComPropApp** which is designed by Cooperative Research Ships (CRS) partners. **ComPropApp** is a specially designed tool for the FSI analysis of composite propellers by doing one-way coupling of the BEM-FEM solvers. The Boundary Element Method (BEM) solver of **ComPropApp** gives it an edge over Reynolds Averaged Navier Stokes Equations (RANSE) solvers in terms of computation time and cost. Hence, it is suitable for the initial design stage.*

*The validation of calculations is done by using **FebHeli**; a propeller's geometry which is used in the French Research Project. The project is divided into four steps. In the first step, a new blade scantling is defined, as FabHeli's actual scantling can't be used for confidentiality reasons, and the propeller's geometry is reconstructed based on the given input data and new scantling. In the second step, the FSI analyses are carried out by using the one-way and two-way coupling of the RANS-FEM solvers (**STAR-CCM+** **FEMAP**) and **STAR-CCM+**, respectively. In the third step, the FSI analysis is carried out by using **ComPropApp**. Finally, the calculated values of stresses, displacement, and forces from both methods are compared and the conclusion is drawn.*

1 INTRODUCTION

Propeller is one the principal propulsion devices in a marine vessel. It has a rotating hub and blades which are set at a pitch to form a helical spiral. The blades' rotation is converted into thrust by creating a pressure difference. The pressure difference accelerates the fluid mass in one direction and the vessel moves in the opposite direction. Composite materials have numerous applications in various industries because of their properties. Recently, the use of composite material has increased in the marine architecture industry to fabricate not only the ship's structure but also the propellers. A propeller is a critical component to determine the performance and efficiency of a vessel. The composite propellers have technological advantages over conventional metallic propellers, e.g. manganese-nickel-aluminum bronze (MAB) and Nickel-Aluminium-Bronze (NAB), because of their properties such as lightweight, corrosion-resistant, better acoustic damping, reduced cavitation, and pressure fluctuations, reduced magnetic interference, reduced maintenance cost, increased efficiency and lifetime of the propulsion system (Hull (1994); Yamatogi et al. (2009); Paik et al. (2013)). Besides all of these benefits, the flexibility and load-bearing capacity of the propellers can be improved by aligning the fibers in a specific way. It allows the propeller to automatically adjust its shape according to the flow conditions and rotational velocity to avoid fluttering (Young et al. (2016)). All of these properties are captivating for industry and extensive investigation is being carried out in both the academic and industrial sectors. Researchers are working in the field of composite propellers by developing novel materials, increasing the performance by improving the scantling and optimizing the designs to improve efficiency (Vardhan et al. (2019)). Some of the existing designs of the composite propellers are shown below in Fig. 1(NK; Gpr):



(a) Nakashima Propeller



(b) Greenprop

Figure 1: Composite propellers

The significance of the composite marine propellers cannot be denied. Hence, it is essential to develop standardized tools and techniques for the design assessment and validation of this type of propeller.

To predict the hydrodynamic loads on the propeller is important for the structural and performance aspect. Usually, model tests are performed to evaluate the performance of the propellers experimentally. The experimental evaluation of propeller is a costly and time consuming process, therefore, suitable numerical models are preferred. The Boundary Element Method (BEM) and Reynolds's Averaged Navier Stokes Equations (RANSE) are the most commonly used numerical methods to predict the hydrodynamic loads on the propeller. The BEM approach is based on potential flow theory, whereas, RANSE is based on the solution of averaged Navier Stokes equations. BEM solvers are fast but less accurate while RANSE solvers are time consuming but more accurate. In this study these two approaches are used to predict the loads on the propeller and the obtained results are compared.

The structural analysis of the propeller is challenging because of the complex loading conditions and geometry. There are two basic approaches for the propeller's structural analysis; analytical methods and numerical analysis. The analytical methods include Taylor's method, curved beam, plate, and shell theories, and Rösingh formulation, etc. Cohen (1955) while the numerical approach uses FEM solvers to compute the displacement and stresses numerically (Atkinson (1968)). Recently, researchers (Paboeuf et al. (2018)) of the classification society Bureau Veritas (BV) have developed an analytical approach specific to the composite propellers. This approach is based on the Cantilever Beam Method (CBM) and gives considerably close results to the numerical ones. The

analytical methods are simple, easy to apply and gives solution much faster than numerical methods. However, the solutions are less accurate because of the assumptions made to simplify the problem. On the other hand, computationally, numerical methods are time-consuming and costly but they are more accurate.

The properties of composite propellers differ from the conventional metallic propeller in many aspects. Among all the properties, the elastic behavior of the composite propeller is most crucial for modelling to perform the numerical analysis. Conventional metallic propellers are considered as a rigid structure in numerical analysis because of their high elastic coefficient values. Therefore, their thrust performance can be evaluated by lifting surface theory (LST) and Computational Fluid Dynamics (CFD). In the case of composite propellers, the value of the elastic coefficient is lower and they deform due to fluid loads. This deformation changes the performance of the propeller, hence, fluid analysis alone is not sufficient to predict the performance. Therefore, for the accurate prediction of the composite propellers' performance, the fluid analysis must be coupled with structural analysis for the simultaneous calculation of loads and stresses. This coupling is known as fluid-structure interaction analysis (FSIA) (Motley et al. (2009)). In this study different types of FSI techniques are used and compared to predict the structural performance of the propeller.

1.1 Propeller's Geometry

The coordinates of the propeller can either be defined in the Cartesian coordinate system or polar coordinates system. Internationally, different coordinates systems are used to define propeller's geometry as there is no defined standard reference system (Munthe-Kaas (2018)). The propeller has two parts; the hub and blades. The basic geometrical parameters of a propeller blade are the propeller diameter (D or $2R$), the number of blades (N), blade's chord length (C), the maximum blade's thickness (t), the blade's camber (f), the rake (Z), blade's pitch (P), the pitch angle (ϕ), the skew angle (θ) and blade's surface offset while the hub or boss has a diameter (d) and length (l). Some of the defined parameters are shown in the Fig.2 (Bertram (2011)).

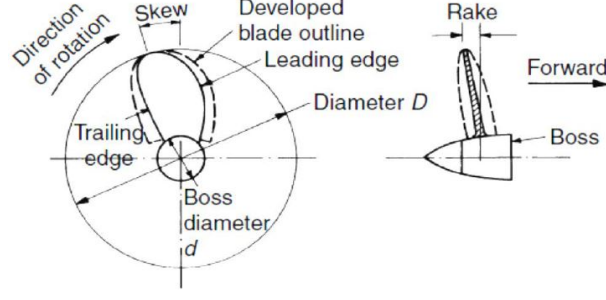


Figure 2: Propeller's geometry parameters

The diameter of the propeller is equal to the diameter of the circle which is formed when a propeller rotates. The design parameters of the propeller are given in radial sections. The radial blade section is defined as the blade section along the circumference of the imaginary cylinder which radius is equal to the radius of the section it is passing through (Carlton (2018)). The radial section is demonstrated in the Fig.3. Here, X shows the axis of the shaft line, Z axis is taken positive in a downward direction, r shows the radius of the imaginary cylinder, whereas the blade section along the cylinder's surface is highlighted in black. For every cylinder defined at different blade sections, a helix can be formed along the cylinder's surface which is developed through the leading and trailing edge. The helix line for one of the blade's radial section is demonstrated in the Fig.3 (Carlton (2018)).

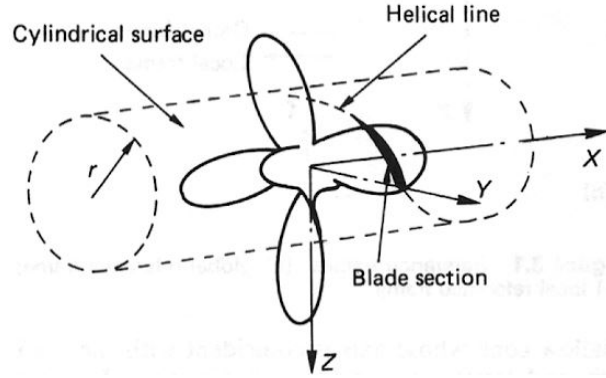


Figure 3: Demonstration of the helix line

The radii of the sections are defined as the ratio section radii (r) and propeller's radius (R) i.e. $r/R = [0.2, 0.3, 0.4, 0.5, 0.6, 0.7, 0.8, 0.9, 1]$. The design parameters are defined in the expanded view or opened out the view. The imaginary cylinder is unwrapped into a plate rectangular plane and then the blade sections are defined in flat XY -plane. The expanded section is demonstrated in the Fig.4 (Carlton (2018)).

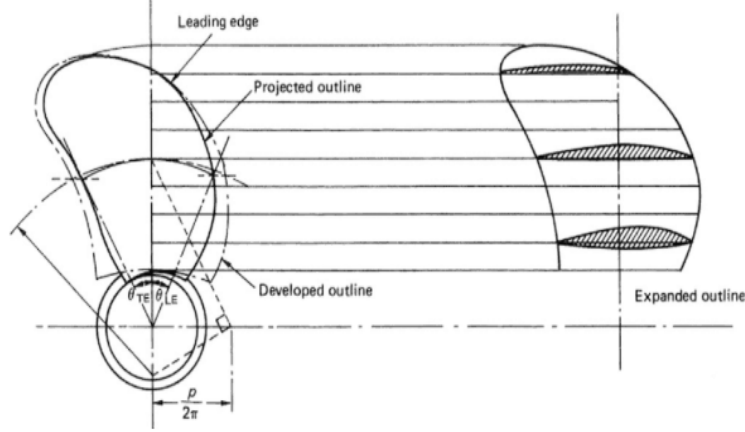


Figure 4: Expanded view of the propeller's blade

Here the left-hand shows the original cylindrical section of blade at different radii while the right-hand shows the expanded view of the blade sections. The pitch is defined as the linear distance that a blade's section covers along X-axis after completing one rotation. In the expanded view, the above-defined helix line is converted into the diagonal of the rectangular section. The pitch of the blade is defined in Fig.5 (Carlton (2018)).

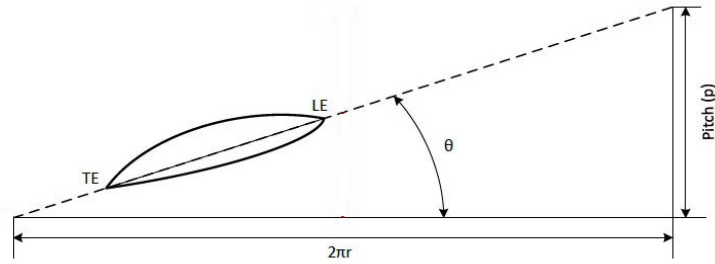


Figure 5: Propeller's blade pitch

Here, LE and TE are leading edge and trailing edge respectively. The line segment joining LE with TE is the chord length of the blade. As the cylinder is transformed into a rectangular plane, the circumference of the cylinder is expanded along Y direction while the pitch distance gets expanded along X direction. The relation for the pitch angle can be derived as follow:

$$\theta = \tan^{-1}\left(\frac{P}{2\pi r}\right) \quad (1)$$

Pitch is a significant design parameter as it determines the blades angle of attack and the pressure exerted on and by the blade. It has a great impact on the efficiency of the blade.

A blade is formed by stacking different sections of the hydrofoil. The blade's thickness may not be uniformly distributed across the chord line, therefore, it creates a camber in the propeller blade. Some of the parameters of the hydrofoil are shown in Fig.6 (Carlton (2018)).

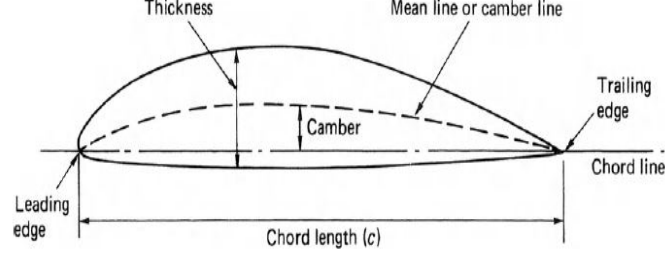


Figure 6: Hydrofoil geometry

1.2 Propeller Performance Characteristics

The propeller performance characteristics are divided into two cases; open water and behind-hull properties. The performance is expressed in the following non-dimensional terms (Carlton (2018)):

- Thrust coefficient K_T

$$K_T = \frac{T}{\rho n^2 D^4} \quad (2)$$

Where, T is the thrust (N), ρ is density (kg/m^3), n is revolutions per seconds RPS and D is diameter (m).

- Torque coefficient K_Q

$$K_Q = \frac{Q}{\rho n^2 D^5} \quad (3)$$

Where Q is torque on the propeller shaft (Nm).

- Advance coefficient J

$$J = \frac{V_a}{nD} \quad (4)$$

Here, V_a is the advance velocity of the vessel.

- Cavitation number σ

$$\sigma = \frac{p_o - e}{0.5\rho V^2} \quad (5)$$

Here, p_o is reference pressure, e is the vapour pressure of the water and V is representative velocity that can be based either on free stream velocity, local velocity or propeller's rotational speed.

- The efficiency of the propeller is defined as:

$$\eta_0 = \frac{K_T}{K_Q} \frac{J}{2\pi} \quad (6)$$

1.3 Objectives

The research work is done as a part of CRS project known as COMPROP2. COMPROP2 is about the development of a specially designed tool (ComPropApp) for the FSI analysis of composite marine propellers. The validation is done by performing FSI analysis by means of commercial RANSE solver (STAR-CCM+) and FEM solver (FEMAP) for only one inflow velocity of the open water case which is 10.3 m/s. The fluid solver of ComPropApp (PROCAL) is a Boundary Element Method (BEM) solver that is based on the potential flow theory while the structural solver (TRIDENT) is an FEM solver. The propeller used in this study is known as FabHeli which is developed under a French Research Project. It is partly funded by Direction Générale de l'Armement (DGA), led by LoireTech and partners are Naval Group and Meca in collaboration with ALM and Bureau Veritas. The figure below shows the shape of the propeller:



Figure 7: FabHeli Propeller

The characteristics of FabHeli are as follow:

Table 1: Characteristics of FabHeli

1	Diameter (D)	1.10 m
2	Blade number (N)	5
3	Material	Carbon Fibers and Vinylester
4	Hub connection type	Bolted

1.4 Organization of the Project

The project has several different steps which are as follow:

- The first step is to define new scantling for the propeller according to the class rules i.e. BV NR546 and to reconstruct the geometry according to the input values. The original scantling of FabHeli cannot be used as it is confidential. The FSI analysis is done for two cases; the isotropic steel blade and the composite blade. The details are discussed in the second chapter.
- The second step is to setup a CFD model by using commercial Reynolds Averaged Navier Stokes (RANS) solver (**STAR-CCM+**). In this step, the CFD solver is coupled with the FEM solver (**FEMAP**). The loads are determined by the CFD solver while the stresses are computed by the FEM solver. In case of isotropic blade, the complete FSI is done by using **STAR-CCM+**. In case of the composite blade, the file-based coupling is done between **STAR-CCM+** and **FEMAP** because the integrated FEM solver of **STAR-CCM+** was unable to model the solid laminates required for the composite modelling. The process is detailed in the third chapter.
- In the third step, the BEM-FEM FSI solver (**ComPropApp**) is used. **ComPropApp** has incorporated BEM solver (**PROCAL**) to calculate the pressure loads and the FEM solver (**TRIDENT**) to calculate the stresses, deformation and forces. The process is detailed in the fourth chapter.
- Finally, the obtained results from **ComPropApp** are compared to the results obtained by FSI analysis done by the RANS-FEM coupling and conclusions are drawn. It is discussed in the fifth and the sixth chapters of the report.

The organization is summarized in the chart below:

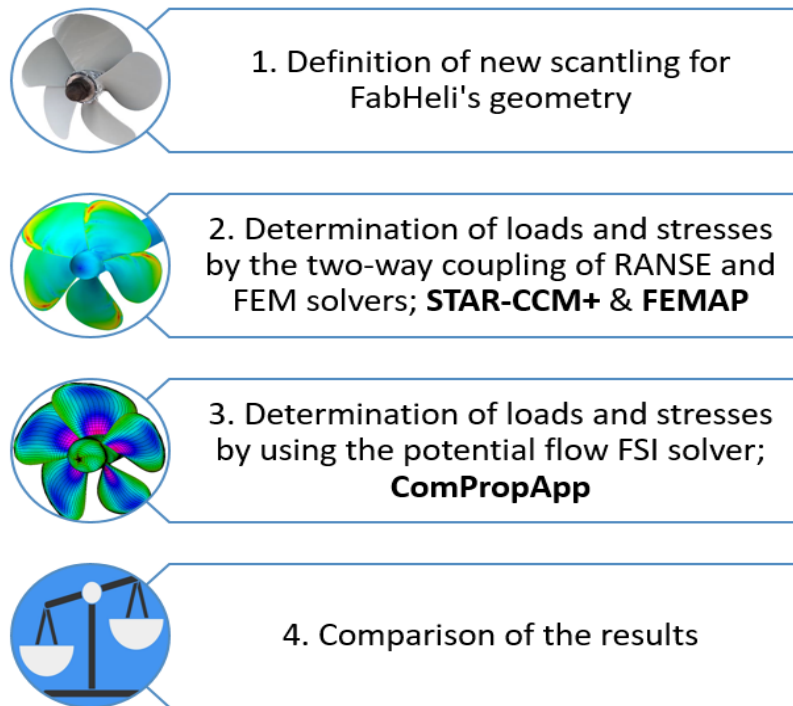


Figure 8: Project organization

2 SCANTLING AND RECONSTRUCTION OF PROPELLER'S GEOMETRY

Composite propellers are manufactured by stacking the layers of fibres, e.g. Glass fibres (GF), Carbon fibres (CF) and aramid fiber (AF) etc., using resins such as Epoxy, Vinylester, Polyester, with a core in between them. Generally, the directions of fibers' orientation θ in the face-sheet laminates are 0° , $\pm 45^\circ$ and 90° . Hence, to optimize a composite panel, it is required to determine the suitable laminate stacking sequence and direction while meeting the criteria and respecting the constraints (Bir et al. (2012)). The sequence of layers can either be symmetric or asymmetric about the midplane. If the sequence and properties of layers are the same on both sides of the middle plane then it is known as symmetric laminate, otherwise, it is asymmetric laminate. Similarly, the stacking sequence can be balanced and unbalanced. If the plies have the same equal numbers of $-\theta$ and $+\theta$ then it is termed as balanced laminate, otherwise, it is unbalanced laminate. The different configurations of stacking sequences are demonstrated in Fig.9 (Hull (1994)).

Unbalanced Asymmetric	Unbalanced Symmetric	Balanced Asymmetric	Balanced Symmetric
0	0	0	0
90	90	60	60
	90	120	120
	0		120
		0	60
		60	0
		120	
		0	0
		60	135
		120	90
			45
			45
			90
			135
			0

Figure 9: Laminates stacking sequences

Many researchers have carried research by using different combinations of different composite materials, different stacking patterns and the different number of layers. The arrangement of fibres in a specific direction enables the blade to twist under the bending moment. The two primary mechanisms to improve the performance of the composite marine propellers are bending-twisting coupling effects of an-isotropic composites and self-adaption behavior depending on the load (Motley et al. (2009)). The bending-twisting coupling affects the performance and efficiency of the propeller as it is linked with thrust

and torque.

The optimal stacking sequence is significant for the blades' performance. It is found that the symmetrical laminates have higher bending stiffness than asymmetric laminates

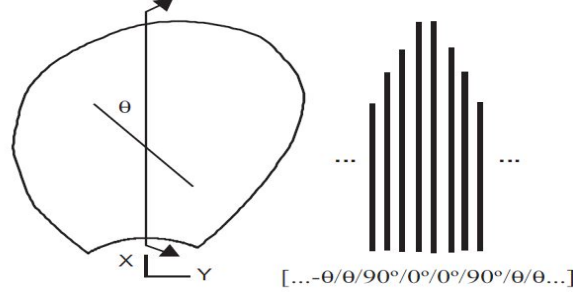


Figure 10: Laminates stacking sequences

They found that the stacking sequence influences the deflection of the blade, therefore, it is directly linked to the thrust and pitch ratio; especially in the case where advanced coefficients are low. They also found that thrust changed in case of the unbalanced stacking sequence. Lin et al. (2005) evaluated the strength of the previously mentioned blade (Lin et al. (2010)) by considering five failure modes: fibre tension, fibre compression, matrix tension, matrix compression, and blade delamination by using different fibre orientations; [.../-45₂/90/0]_s, [.../θ₂/90/0]_s and [.../-15/15/90/0]_s. They also did the nonlinear hydrostatic analysis and found that fibre orientation [.../-45₂/90/0]_s had insufficient structural strength while the other two orientations were fine.

Kishore and Behera (2015), studied the natural frequencies of the composite blade by using different laminates. They found that laminate properties directly affect the dynamic behavior of the blade.

2.1 Design Guidelines for the Laminates

Designing of laminates starts by selecting ply angles suitable for the given application. The next steps include the selection of plies number, the proportion of specific orientation and stacking sequence. The design guidelines for the laminate are based on return on experience (ROE) from testing and analysis. The basic six laminate design guidelines for the stacking sequence, to maximize the structural strength are summarised as follow(Bailie et al. (1997)):

1. **Symmetry:** The stacking sequence should be symmetrical to the mid-plane.

2. **Balance:** The stacking sequence should be balanced. Symmetry and balance guidelines minimize the shear extension and membrane bending coupled behavior of laminate.
3. **Ten percent rule:** A minimum of 10% of plies are required for each direction i.e. 0° , $\pm 45^\circ$ and 90° . It is done to avoid matrix dominated behaviors.
4. **Disorientation:** The orientation difference between two consecutive plies should not exceed 45° . The purpose is to reduce unwanted failure modes like free-edge delamination.
5. **Contiguity:** The number of plies stacked together with the same orientation should not exceed a defined value. It should be done to avoid transverse matrix cracking.
6. **Damage tolerance:** A 0° should not be located at the upper and lower surface of the laminate. This is done to shield the primary load-carrying plies from any kind of damage for the exposed surface like scratches etc.

In case of the geometry which has varying thickness, the plies are dropped off at particular locations to maintain the correct thickness at different zones. This complicates the design process because of the formation of resin pockets within the structure. The schematic view of such laminate is shown in Fig.11 (Bailie et al. (1997)).

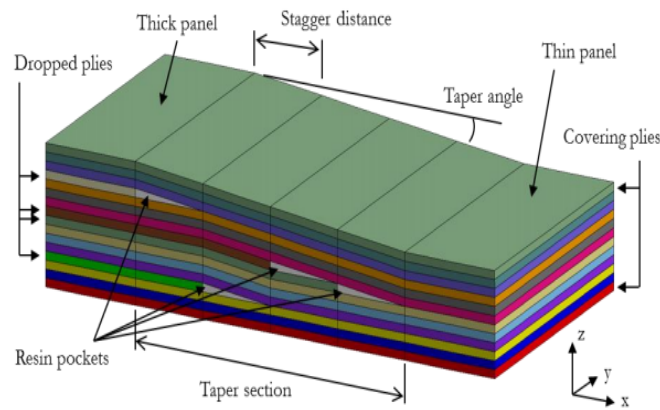


Figure 11: Ply-drop-off in laminate of varying thickness

The guidelines concerning with the design of ply-drop-off are as follow (Mukherjee and Varughese (2001); Lasseigne (2016)):

1. **Covering ply:** The covering plies of the laminate should not be dropped off. It is done to avoid delamination.
2. **Continuity:** All the plies in the thin section must cover the whole structure. The mismatch of ply orientation between two zones/panels, i.e. thick panel and thin panel, is forbidden. This is done for the sake of structural integrity of the structure.
3. **Internal continuity:** Keep the continuous plies between the two consecutive ply-drops.
4. **Ply-drop alternation:** The location of ply-drops should alternate from near to far from the mid-plane of the laminate.
5. **Staggered distance:** Staggered distance should be the eight times of the drop off thickness when 45 plies are dropped.
6. **Δn rule:** This rule specifies the maximum number of ply-drops between adjacent panels. It constraints the thickness variation in adjacent panels which reduces high-stress concentrations.
7. **Taper guidelines:** Laminates in the taper region should comply with laminate design guidelines to the maximum extent.

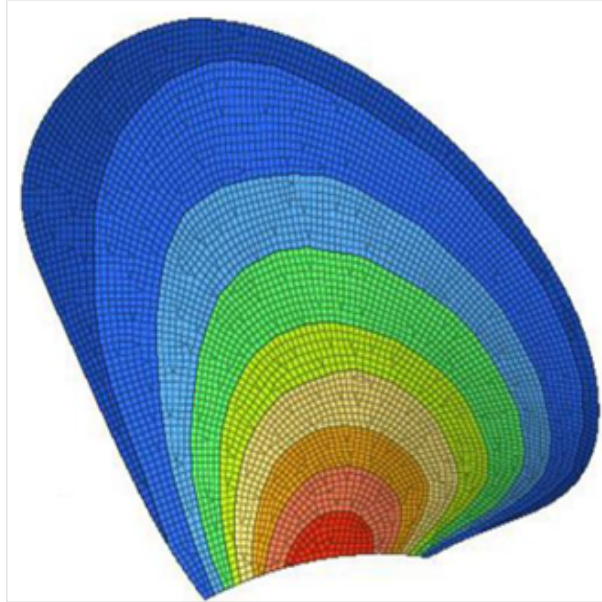
2.2 Blade's Scantling:

A new scantling is designed for the blade according to the design guidelines for laminates and the rules defined by Bureau Veritas in their rule book for composites known as NR546 (Veritas (2018)). Each layer has HS Carbon fibres and Vinylester resin. The laminate is formed by stacking the layers of unidirectional layers (UD) and woven roving at different angles. In unidirectional layers, the fibres are oriented along one direction, whereas, in woven roving the fibres are oriented in two directions which are perpendicular to each other just like in woven fabric. The properties of unidirectional layer woven roving is shown below in the Table 2:

Table 2: Properties of individual layers

Properties	Unidirection Layer	Woven Roving
Fibre	HS Carbon	HS Carbon
Resin	Vinylester	Vinylester
Volume Percentage of fibre (%)	45	45
Mass/ m^2 of fibre (g/m^2)	600	600
Mass/ m^2 of resin (g/m^2)	450.65	450.65
Mass/ m^2 total (g/m^2)	1050.65	1050.65
Volume Percentage of fibre (%)	-	50
Thickness (mm)	0.745	0.745
Density	1.411	1.411

The blade is divided into nine different zones. The division is shown in the Fig.12. The zones shown in the Fig.12 are not up to the scale and are presented to give an idea. For the sake of understanding only one blade is shown with the corresponding part of the hub attached with it. Each zone has a different laminate with different thickness

**Figure 12:** Division of the blade into nine zones

and property. An in-house software known as **ComposeIT** is used to define the layup properties of each laminate. The layup sequence of the laminates is shown below:

2	32	45	0.74	X	X	X	X	X	X	X	X	X	INTRADOS
1	31	0	0.74	U	U	U	U	U	U	U	U	U	
1	30	0	0.74	U	U	U	U	U	U	U	U	U	
1	29	0	0.74		U	U	U	U	U	U	U	U	
2	28	45	0.74			X	X	X	X	X	X	X	
1	27	0	0.74			U	U	U	U	U	U	U	
1	26	0	0.74				U	U	U	U	U	U	
1	25	0	0.74				U	U	U	U	U	U	
2	24	45	0.74					X	X	X	X	X	
1	23	0	0.74					U	U	U	U	U	
1	22	0	0.74						U	U	U	U	
1	21	0	0.74						U	U	U	U	
2	20	45	0.74							X	X	X	
1	19	0	0.74							U	U	U	
1	18	0	0.74								U	U	
1	17	0	0.74									U	
1	16	0	0.74									U	EXTRADOS
1	15	0	0.74									U	
1	14	0	0.74							U	U	U	
2	13	45	0.74							X	X	X	
1	12	0	0.74						U	U	U	U	
1	11	0	0.74						U	U	U	U	
1	10	0	0.74					U	U	U	U	U	
2	9	45	0.74					X	X	X	X	X	
1	8	0	0.74				U	U	U	U	U	U	
1	7	0	0.74				U	U	U	U	U	U	
1	6	0	0.74			U	U	U	U	U	U	U	
2	5	45	0.74			X	X	X	X	X	X	X	
1	4	0	0.74		U	U	U	U	U	U	U	U	
1	3	0	0.74	U	U	U	U	U	U	U	U	U	
1	2	0	0.74	U	U	U	U	U	U	U	U	U	
2	1	45	0.74	X	X	X	X	X	X	X	X	X	
Layer	No. plies	Angle	Thickness	A1	A2	A3	A4	A5	A6	A7	A8	A9	
Number of plies per zone				6	8	12	16	20	24	28	30	32	
Zone thickness (mm)				4.47	5.96	8.94	11.92	14.9	17.88	20.86	22.35	23.84	

Figure 13: Sequence of the laminates

In the Fig.13, U is for unidirectional fibre, X is for woven roving and the dark blue part in the middle of plies is representing the core which is made of Polymerizing Vinyl Chloride (PVC) form. The core's thickness is adjusted in each zone to match the actual thickness of the blade. The properties of the different laminates are shown below in the Table3.

Table 3: Properties of the laminates used in propeller's scantling

	Thickness	Density	Ex	Ey	Gxy	νx	νy	Vx	Vy	EIx	EIy
	mm		MPa	MPa	MPa			mm	mm	N.mm ² /mm	N.mm ² /mm
A1	4.47	6.304	77 271	13 079	11 419	0.666	0.113	2.235	2.235	3.03E+05	1.33E+05
A2	5.96	8.405	85 412	11 276	9 346	0.619	0.082	2.98	2.98	9.37E+05	3.01E+05
A3	8.94	12.608	77 271	13 079	11 419	0.666	0.113	4.469	4.469	3.89E+06	9.13E+05
A4	11.92	16.81	85 412	11 276	9 346	0.619	0.082	5.959	5.959	9.94E+06	2.04E+06
A5	14.9	21.013	80 534	12 378	10 590	0.649	0.1	7.449	7.449	2.03E+07	3.80E+06
A6	17.88	25.216	85 412	11 276	9 346	0.619	0.082	8.939	8.939	3.61E+07	6.38E+06
A7	20.86	29.418	81 930	12 069	10 234	0.641	0.094	10.428	10.428	5.84E+07	9.90E+06
A8	22.35	31.52	83 789	11 650	9 760	0.63	0.088	11.173	11.173	7.23E+07	1.21E+07
A9	23.84	33.621	85 412	11 276	9 346	0.619	0.082	11.918	11.918	8.83E+07	1.45E+07

3 FSI ANALYSIS BY RANS-FEM COUPLING

Fluid-structure interaction (FSI) is an interdisciplinary subject. It is an important type of multi-physics problem. A problem is termed as multi-physics when it can only be solved by using the laws and equations from different physical disciplines. FSIA is a computational challenge because of intricate geometries and physics but the way of defining the interactions between fluid and structure can reduce the computational effort. FSI can be categorized based on the employed solution procedure (Benra et al. (2011)). These categories are depicted in the the Fig.14:

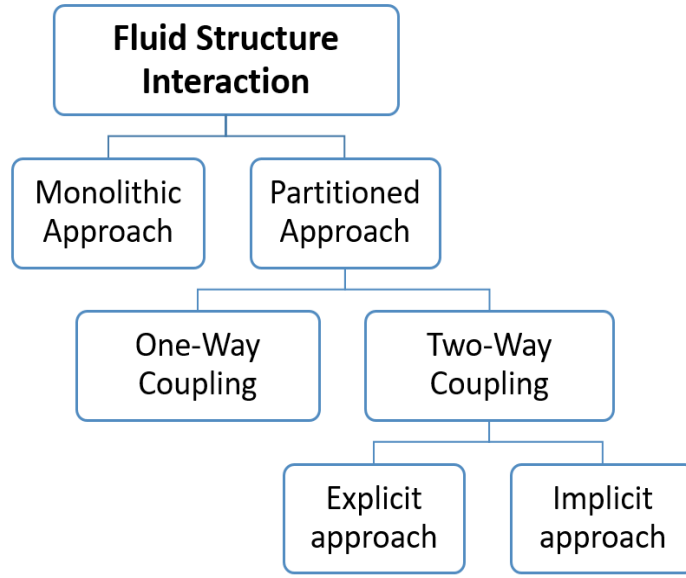


Figure 14: Solution based classification of FSI

In the monolithic approach, both solid and fluid are treated as one unified system and equations of both systems are solved simultaneously. In the partitioned approach, fluid and solid are treated as two different systems coupled with some interface. The difference between monolithic and partitioned approach is shown in the Fig.15 (Benra et al. (2011)).



Figure 15: Two approaches for FSI analysis

Here, Ω_s and Ω_F are structural and fluid solutions, respectively. In the engineering ap-

plications, the partitioned approach is preferred because it allows using independently developed and tested solvers for the fluid and structural analysis. The partitioned approach is further subdivided into one-way and two-way coupling.

In the one-way coupled FSI analysis, at first the fluid analysis is done until convergence then the loads from the fluid are imported to the FEM solver and structural analysis is done until convergence. In this type of coupling the converged solution of fluid field, i.e. the pressure loads from the fluid solver, is transferred to the structural field for once.

In the two-way coupled FSI analysis, the geometry displacement obtained from the structural solver is also imported back in the fluid solver and the fluid analysis is done for the next time step. The process is repeated until the geometry reaches the equilibrium. The two-way coupled FSI analysis is further divided into explicit and implicit approach depending on the way the information is exchanged between the fluid and the structural solvers.

The explicit two-way coupling is also termed as the weak coupling. In the weak coupling, at time step N ;

- The hydrodynamic loads are calculated for deformed geometry mesh obtained from the previous time step.
- The calculated fluid loads are transferred to the structural solver.
- The structure is deformed under the loads obtained from time step N .
- The calculated deformation, on the fluid-structure interfaces, from the structural solver is transferred to the fluid solver.
- The process is repeated until the geometry reaches the equilibrium.

The implicit two-way coupled FSI is also termed as strong coupling. This scheme is considered close to the monolithic approach. The fluid flow solution is converged and the loads are transferred to the structural model by mesh interpolation within one inner time step. The structure analysis is done till convergence and the mesh of the structure deforms under loads. This deformed structure is taken back into the fluid solver where the boundaries between the fluid and structure are interpolated to the fluid mesh and fluid mesh also changes accordingly. This way one inner loop of the iteration is closed. It has following characteristics:

- The variables of fluid and structure domain are synchronized.
- The system of equations used in strong coupling is the same as the one used in the implicit monolithic approach.
- It is already presented that the solution achieved from the strong coupling enables the selection of large time steps, is more stable, ensures better conservation of energy and momentum, and improves solution accuracy (Storti et al. (2006)).

The flow chart of the explicit and implicit two-way coupled FSI are shown below in Fig.16 (Benra et al. (2011)):

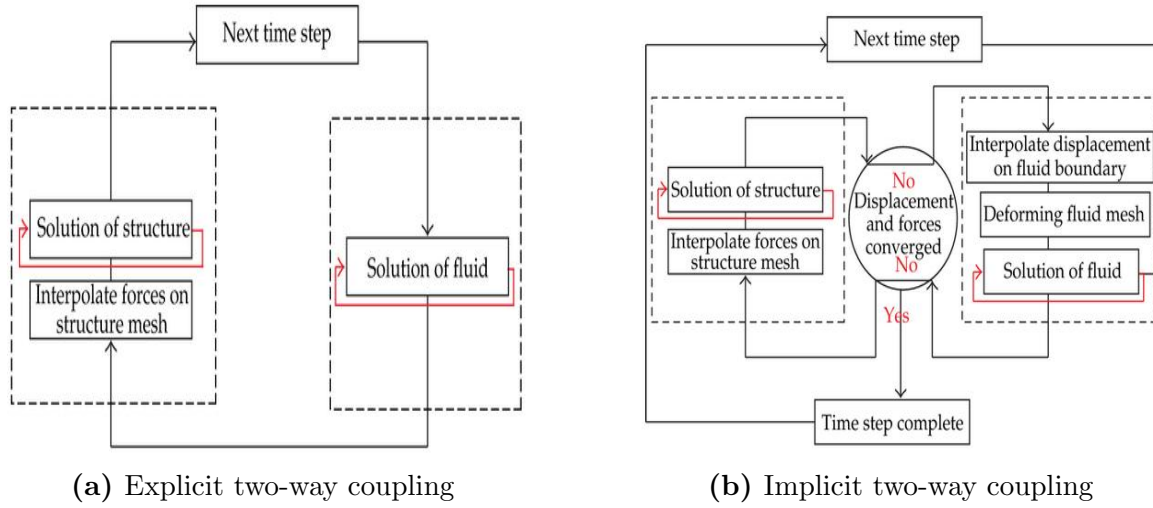


Figure 16: Flow charts of one-way and two-way couplings

The FSI analysis is divided into several categories based on different parameters (Sigrist (2015)).

- In the case of flow physics, FSI is divided into two groups; compressible and incompressible. In the case of water and solid interaction, the incompressible assumption is made while for gases both compressible and incompressible assumptions can be made depending on the physics like Mach number. In the present case, the fluid is water, therefore, the incompressible assumption will be used.
- FSI can also be classified based on the way structure is interacting with fluid; rigid body and deformable body case. Rigid body-fluid interaction is mostly assumed in the case of ships, offshore structures, and water turbines while deformable body-fluid interaction includes aeroelasticity, hydroelasticity and poroelasticity cases. In

both cases, the interaction of the fluid with the body is strongly coupled. In the present case, the blade is deformable.

3.1 Calculations Done by the RANSE Solver

In a fluid solver, the fluid flow is described at every point $P(x,y,z)$ in the Eulerian space. The distribution of velocity and pressure is calculated numerically by using CFD techniques. The flow is described as a vector field in the Cartesian plane and it varies both in space and time (White (2006)). The velocity vector in 3D space is written as:

$$\vec{V}(r, t) = u(x, y, z, t)\vec{i} + v(x, y, z, t)\vec{j} + w(x, y, z, t)\vec{k} \quad (7)$$

In case of incompressible fluid, the divergence of the field is equal to zero.

$$\nabla V = \frac{\partial u}{\partial x} + \frac{\partial v}{\partial y} + \frac{\partial w}{\partial z} = 0 \quad (8)$$

Therefore, the mass conservation or continuity equation can be written as:

$$\nabla \cdot (\rho \vec{V}) = 0 \quad (9)$$

The momentum conservation equation is written as:

$$\rho \left(\underbrace{\frac{\partial \vec{V}}{\partial t}}_{\text{local acceleration}} + \underbrace{\vec{V} \cdot \nabla \vec{V}}_{\text{convective acceleration}} \right) = \underbrace{-\nabla P}_{\text{pressure terms}} + \underbrace{\nabla \cdot \tau_{ij}}_{\text{viscous terms}} + \underbrace{F_b}_{\text{body forces}} \quad (10)$$

In case of Newtonian fluids, the viscous forces τ_{ij} are proportional to the product of coefficient of viscosity and element strain rate. All of the above mentioned equations combined to form Navier Stokes Equation (NSE). To capture turbulent flow by numerically solving NSE requires very fine mesh which is computationally intensive and time consuming. Therefore, instead of using NSE the problem is solved by using Reynolds Averaged Navier Stokes equations (RANSE). In RANSE (Wilcox et al. (1998)), the instantaneous quantities of velocity and pressure are decomposed into fluctuating and time averaged components. Let u is an instantaneous velocity component then it can be writ-

ten as follow:

$$u_i(t) = \underbrace{\bar{u}_i}_{\text{Time-averaged term}} + \underbrace{u'_i}_{\text{Fluctuating term}} \quad (11)$$

The momentum conservation after Reynolds averaging is written as:

$$\rho \left(\frac{\partial \bar{u}_i}{\partial t} + \bar{u}_j \frac{\partial \bar{u}_i}{\partial x_j} \right) = - \frac{\partial \bar{P}}{\partial x_i} + \mu \frac{\partial^2 \bar{V}_i}{\partial x_j \partial x_j} - \rho \frac{\partial u'_i u'_j}{\partial x_j} + \rho F_b \quad (12)$$

Here, $\frac{\partial u'_i u'_j}{\partial x_j}$ is an additional unknown term called Reynolds stresses. To close the equations, Reynolds stresses must be modelled by equations of known quantities. In 1877, Boussinesq (Boussinesq (1877)) proposed a formula for Reynolds stresses based on molecular viscosity theory which is given as follow:

$$- \rho \bar{u'_i u'_j} = \tau_{ij} = \mu_t \left(\frac{\partial \bar{u}_j}{\partial x_i} + \frac{\partial \bar{u}_i}{\partial x_j} \right) - \frac{2}{3} (pk + \mu_t \frac{\partial \bar{u}_k}{\partial x_k}) \delta_{ij} \quad (13)$$

Where, μ_t and k are turbulent viscosity and turbulent kinetic energy respectively. Turbulent viscosity should be modelled again to close the system of equations. The most frequently used model for this purpose are known as the two-equation eddy viscosity models which are $k - \epsilon$, $k - \omega$, and SST models. The two-equation models have two partial differential equations; one for the turbulence length scale and the other for the turbulent velocity scale. In this report, only steady flow simulations are performed.

The CFD software used in this project is STAR-CCM+ which is a RANSE solver. It is capable of handling intricate geometries and complex physics as it includes innovative meshing techniques and the latest physical models. It uses the Finite Volume Method (FVM) along with the turbulence closure models to solve RANS equations in the integral form.

3.2 Geometry Preparation

It is important to define the fluid domain before running the simulation. The symmetrical fluid domain was defined for one blade and a part of the hub. This is done to reduce the computational time and power. The propeller's blades are overlapping each other, thus, defining the domain such that it only covers one blade was not obvious. The software used for this purpose is **Rhinoceros 3D**. The created Moving Frame of Reference (MRF)

is shown below:

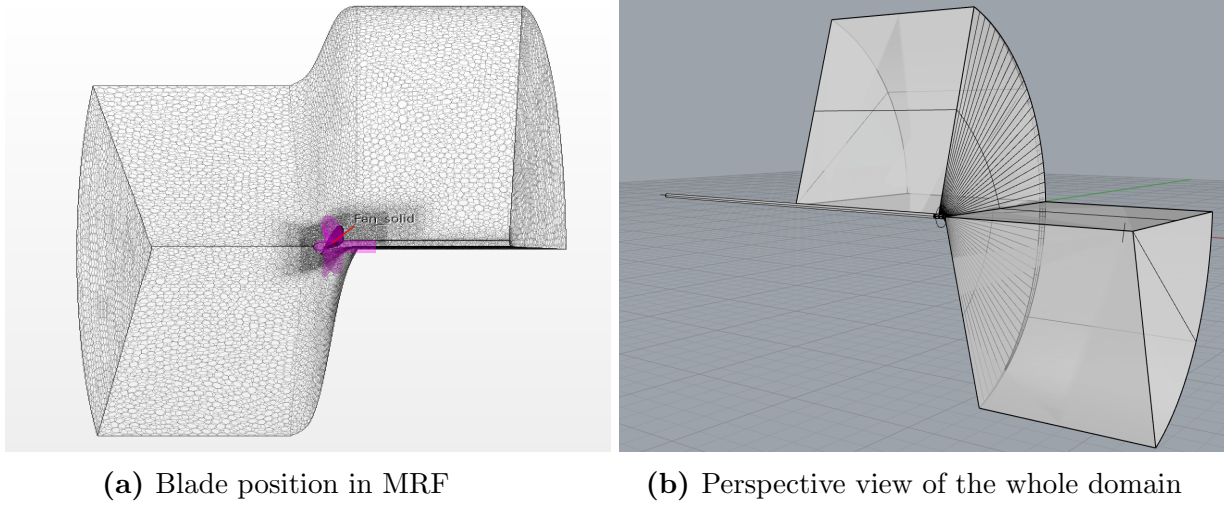


Figure 17: Propeller in fluid domain

The domain is split into two parts; each covering the half of the blade and then it is rotated at 75 degrees. The user defined parameters in the software are shown below:

Table 4: Defined parameters in STAR-CCM+

	Parameter	Value
1	Inflow Velocity (m/s)	10.3
2	Propeller rotation (rev/s)	12.19
3	Density of water (kg/m^3)	1030

3.3 Calculations Done by the FEM Solver

The linear static analysis is carried out using a commercial FEM solver known as NAS-TRAN which is integrated in FEMAP while FEMAP is used to pre-process and post-process the data. In the FEM solver, the geometry is discretized into finite elements by using solid laminate elements which allow ply-by-ply analysis. The ply-by-ply analysis does stress calculation for every layer of the laminate, therefore, the reason of the failure can be understood in a better way. The geometry is discretized by using hexahedral mesh. The mesh is generated in TRIDENT and then exported in FEMAP because TRIDENT is capable of generating structured mesh with ease. Special attention is paid to use the similar FEM models in two different FEM solvers (FEMAP and TRIDENT) to minimize the discrepancies associated with the dissimilarities. Adequate mesh size is significant

for the accuracy of the results, therefore, a mesh convergence study is carried out by using isotropic material. The Table8 below shows the displacement and Von Mises stress obtained for different element numbers.

Table 5: FEM mesh convergence study

Element no.	Displacement (mm)	Von-Mises Stress (MPa)
40 x 40	1.39	52.1
50 x 50	1.39	51.9
70 x 70	1.39	51.9
90 x 90	1.4	51.8
100 x 100	1.4	51.8
120 x 120	1.4	51.8

The model with 50 x 50 element numbers is selected for the further study after comparing the values of obtained displacements and stresses. The relative difference of the 50 x 50 elements model with the 120 x 120 elements model is only -0.71% in terms of displacement while it is 0.19% in the case of stresses. Although, the relative difference of 70 x70 model is same as 50 x 50 but still 50 x 50 model is selected because the analysis time taken by the later one is least.

The 50 elements model has 50 cells in chordwise direction and 50 elements in radial direction. The mesh used in the both FEM solvers is shown in the Fig.18.

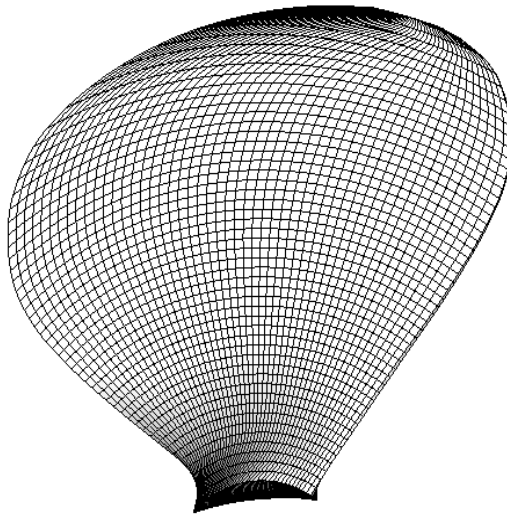


Figure 18: Mesh generated by FEM solver

The displacement of the nodes of the elements is calculated by the following equation:

$$[F] = [K] * [U] \quad (14)$$

In the above equation, F is the force matrix, K is the stiffness matrix and U is the displacement matrix. The force matrix is calculated from the pressure obtained from the CFD calculation while the stiffness matrix depends on the material and geometry of the propeller. The Degrees of freedom (DOF) at the connection of the blade with the hub are suppressed by fixing the nodes at the blade's root.

4 FSI ANALYSIS BY BEM-FEM COUPLING

ComPropApp does FSI analysis by explicit two-way coupling of the fluid solver and the FEM solver. ComPropApp is an in-house tool developed by the CRS community. It is specially designed for the hydro-structural analysis of the flexible (composite) ship propellers. The software has incorporated a coupling algorithm based on Quasi Newton-Inverse Least Square (ILS), whereas it requires a fluid model from a BEM solver (ProVise) and a structural model from a FEM solver (TRIDENT). The propeller's geometry is generated by using .PPG file format which contains the information related to the radial and chord sections of the blade. In this study, the .PPG file is generated by scanning the actual propeller's geometry. The user interface of ComPropApp is shown below in Fig.19 (Wijngaarden (2020)).

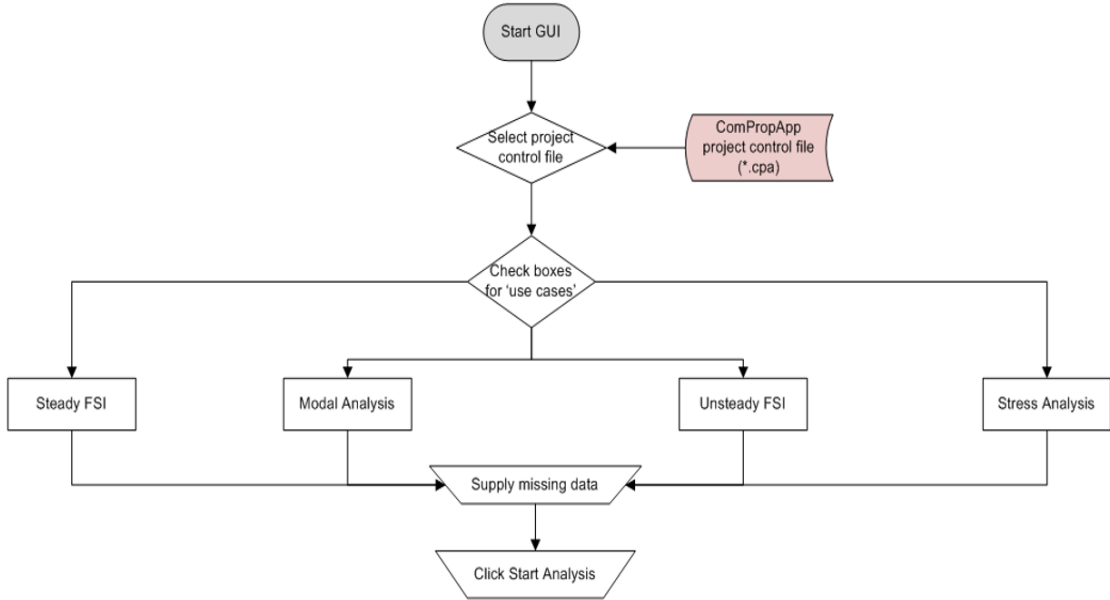


Figure 19: User interface of ComPropApp

To allow large blade deformations, the steady FSI problem is solved by taking into account the geometrical non-linear behavior. Finite Element (FE) solver (TRIDENT) solves this non-linear problem iteratively by applying the actual external blade load incrementally. The user chooses some load increments and loop iterations, say N and M (with $M \geq N$), and the program applies N iterations to arrive at the full load, followed by another M minus N iterations to allow the deformed shape to converge at the maximum load. The starting load (at increment 1) is determined by decreasing the targeted ship speed and RPS in such a way that the advance coefficient remains unaltered and the thrust is

decreased by a factor of N . This information is written to the control file of the boundary element method solver (PROCAL). The external load for the latter case is determined by calling PROCAL. Then, the program EXTPROPTEC is called to interpolate PROCAL's load output to radial stations corresponding to those at which the propeller geometry is defined. At these radial stations, the load is applied to the structural mesh model of finite element method solver (TRIDENT). The whole process is summarised in the flow chart below Fig.20 (Wijngaarden (2020)).

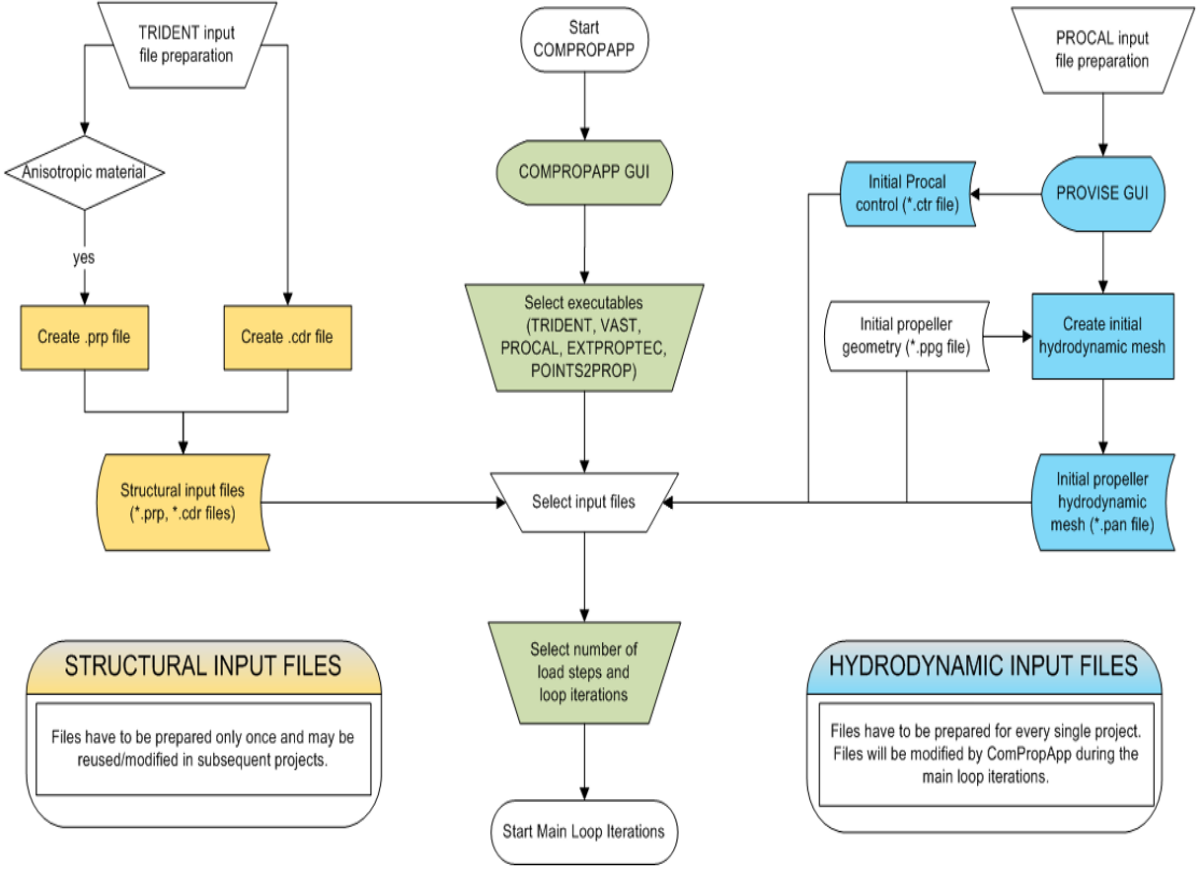


Figure 20: Process flow chart of BEM-FEM coupling

4.1 Calculations Done by the BEM Solver

Boundary element method (BEM) is a numerical computation method to linear partial differential equations which are formulated as integral equations. This method is based on the potential flow theory. Under potential flow theory, the fluid is assumed to be inviscid, isovolume and irrotational. To understand the governing equations of the flow field, assume a three-dimensional closed surface S which is composed of the blade and

hub S_B , the wake S_w , the outer surface S_∞ and a normal vector \vec{n} projecting towards the flow. The general notation for the application of Green's theorem, in case of a propeller rotating in an incompressible, inviscid and irrotational flow of velocity V_∞ is shown below Fig.21 (Lee et al. (2014)).

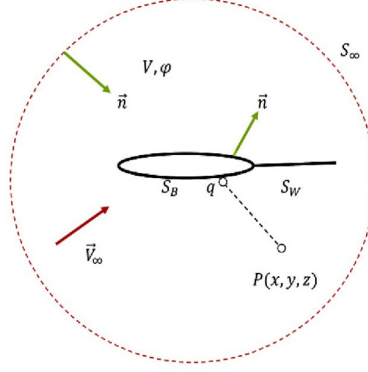


Figure 21: General notation for Green's theorem application

In BEM, the flow is represented as the summation of background velocity V_∞ and perturbation potential gradient ϕ , which satisfies the Laplace's equation.

$$\left. \begin{aligned} V_t &= V_\infty + \Delta\phi \\ \nabla^2\phi &= 0 \end{aligned} \right\} \quad (15)$$

The first boundary condition is the kinematic boundary condition which states that the body is impermeable. This condition must be satisfied on the propeller's blade surface. It is given as follow:

$$\frac{\partial\phi}{\partial n} = -V_\infty n \quad (16)$$

This boundary condition specifies the source strength for each panel as the normal vector and the free stream velocity are known. For behind-ship conditions, the free-stream velocity depends on the angular position and radius of the panel and the source strength thus also depends on the angular position and radius. In steady flow computations, a circumferential averaged ship wake field is used, in which the free-stream velocity thus only depends on the radial coordinate of the collocation point:

$$\sigma = -\vec{n}V_\infty = -\vec{n}(V_W + \omega \times x) \quad (17)$$

The wake surface is assumed to have zero thickness to avoid normal velocity discontinuity.

$$\sigma = \frac{\partial \phi}{\partial n_{Sw}} = \left(\frac{\partial \phi}{\partial n}\right)_{SS} - \left(\frac{\partial \phi}{\partial n}\right)_{PS} = 0 \quad (18)$$

The second condition is the Kutta condition which is applied to make the velocity finite at trailing edge and the outer boundary.

$$\left. \begin{aligned} \Gamma &= -\pi c V_\infty \sin \alpha \\ |\Delta \phi|_{T.E} &< \infty \end{aligned} \right\} \quad (19)$$

The perturbed velocity induced by the propeller vanishes as it proceed away from the surface.

$$\delta \phi \rightarrow 0, \text{ as } r \rightarrow \infty \quad (20)$$

The perturbation potential can be expressed by using Green's second identity for all points on the blade's surface is expressed as:

$$2\pi \phi_p = \int \int_{S_B} \phi_q \frac{\partial}{\partial n_q} \left(\frac{1}{R(p,q)} \right) ds - \int \int_{S_B} \left(\frac{\partial \phi}{\partial n} \right)_q \frac{1}{R(p,q)} ds + \int \int_{S_w} (\delta \phi)_q \frac{\partial}{\partial n_q} \left(\frac{1}{R(p,q)} \right) ds \quad (21)$$

In above mentioned equation, S_∞ is equal to the summation of S_{Blade} and S_{Hub} , p is the influenced point and q is the influencing point where singularity is located while $R(p,q)$ is the distance between p and q . Eq. 21 demonstrates the velocity potential as the distribution of dipole strength of ϕ and source strength of $\partial \phi / \partial n$ on the surface of the blade S_B and $\Delta \phi$ on the surface of the trailing vortex S_w . The source strength $\partial \phi / \partial n$ is obtained from the kinematic boundary condition while the dipole strength ϕ is obtained by simultaneously solving Eq.18 and Eq.19. The geometry is discretized into panels to solve the equations numerically.

$$\sum_j a_{i,j} \phi_j + \sum_m (\Delta \phi)_m W_{i,m} = \sum_j b_{i,j} \sigma_j \quad (22)$$

Here, the effective coefficients $a_{i,j}$ and $b_{i,j}$ are the velocity potential at the i^{th} panel which is induced by the source distributed at j^{th} panel. $W_{i,m}$ is the wake effective coefficient which is the velocity potential located at i^{th} panel and it is induced by the source distributed at m^{th} panel. $(\Delta \phi)_m$ is the potential difference between the upper and lower

side of the trailing edge while σ_j represents the source strength. To solve the integral equation numerically, the surface of the geometry is discretized and approximated by the quadrilateral elements. It is important to have a proper smooth surface grid to avoid numerical errors. Therefore, a fine grid is generated in the BEM solver (Prowise) by discretizing the blade into 50 panels from LE to TE and 50 panels from root to tip. The discretized geometry is shown in the Fig.22 and Fig.23.

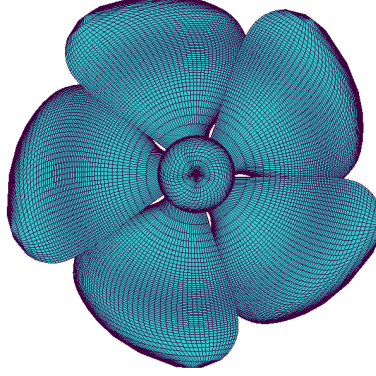


Figure 22: Panel discretization of the propeller

To model trailing edge vortex wake, it is important to apply Kutta condition. When the propeller is rotating, a classical model of wake is generated. In the present case,

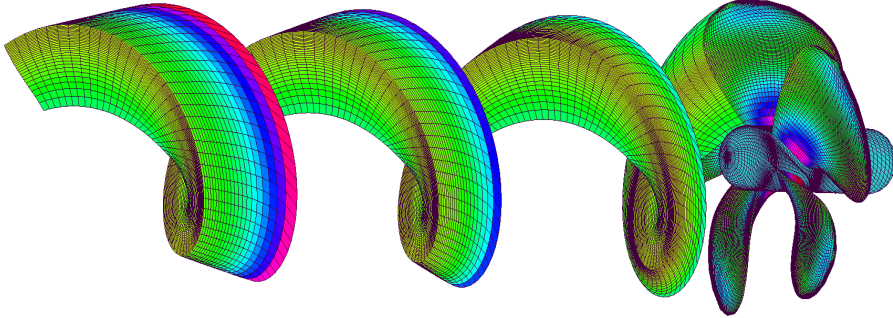


Figure 23: Blade and wake discretization in Prowise

the simulation is run for the steady case. The flow field induces pressure on the blade's surface which is obtained by using the velocity potential derived from the discretized integral equations:

$$C_P = \frac{P - P_\infty}{0.5\rho U_\infty^2} = -\frac{2}{U_\infty^2} \frac{\partial \phi}{\partial t} + \frac{V_F^2}{U_\infty^2} - \frac{|\nabla \phi|^2}{U_\infty^2} - \frac{2V_F \nabla \phi}{U_\infty^2} \quad (23)$$

Finally, the calculated pressure is used to calculate the total thrust and torque.

5 ISOTROPIC BLADE CASE

At first, the FSI analysis is carried out by using isotropic material before proceeding with composite blade. The material used for the isotropic analysis is steel. The Table6 below shows the material properties.

Table 6: Material Properties

1	Young Modulus (E)	200 GPa
2	Density (ρ_{steel})	8060 kg/m^3
3	Shear Modulus (G)	76.9 GPa

The FSI analysis performed by using steel blade is further divided into four cases depending on the type of the solver and FSI method. The flow charts shown below in the Fig.24 shows the different analyses performed for this case.

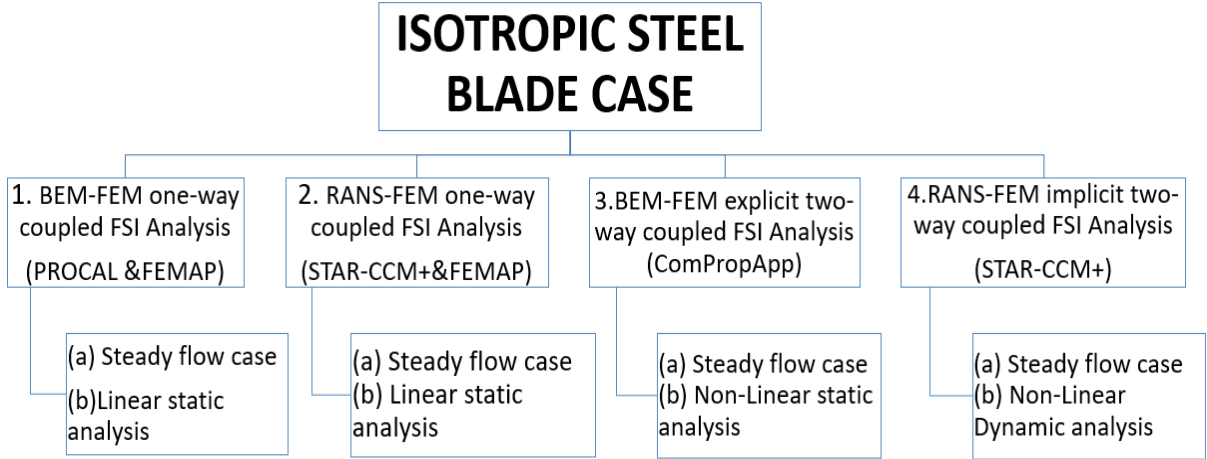


Figure 24: Analysis performed for the isotropic blade case

5.1 Case 1: BEM-FEM One-Way Coupled FSI Analysis

In the first case, the fluid loads generated by the BEM solver (PROCAL) after performing the first iteration of FSI analysis in ComPropApp which are then imported in the commercial FEM solver (FEMAP). The same structure model is used in FEMAP and TRIDENT. The characteristics of this analysis are as follows:

- The steady flow analysis is performed by the BEM solver (PROCAL).
- The fluid loads are imported in FEMAP and linear static analysis is performed.

5.2 Case 2: RANS-FEM One-Way Coupled FSI Analysis

In this analysis case, the FSI analysis is performed by one way coupling of STAR-CCM+ and FEMAP. The fluid and structure models are separately created and solved up to convergence in STAR-CCM+ and FEMAP, respectively. After convergence of the fluid results the loads are imported from STAR-CCM+ to FEMAP and the structural analysis is carried out in FEMAP to obtain the deformation and stresses. The process of importing loads from fluid solver to FEM solver is done only once, therefore, it is classified as one-way coupled FSI analysis. The characteristics of this analysis are as follow:

- The steady flow analysis is performed by the RANS solver (STAR-CCM+).
- The fluid loads are imported from the RANS solver and the linear static analysis is performed by FEMAP.

This is also known as file based coupling. The process to carry this kind of analysis is explained below:

1. The fluid model is generated in STAR-CCM+ and it is solved up to convergence.
2. The initial structural mesh is imported into STAR-CCM+ from FEMAP in such a way that it fits the fluid model.
3. The pressure loads from the face of the fluid volume mesh (cells) are mapped on the face or vertex of the structure mesh by using least square interpolation method.
4. After mapping, the structure model is imported back into FEMAP where material properties and boundary conditions are applied before solving the model.

This process has less accuracy than the implicit two-way coupled FSI analysis as the mapping of loads is done by interpolation. The purpose to perform this case is to compare the difference of the results obtained by implicit two-way FSI analysis.

5.3 Case 3: BEM-FEM Explicit Two-Way Coupled FSI Analysis with ComPropApp

In this analysis case, the complete FSI analysis is performed by ComPropApp. The characteristics of this analysis are as follow:

- The steady flow analysis is performed by the BEM solver (PROCAL).
- The loads are transferred from the fluid mesh to the structure mesh.
- The non-linear static analysis is performed by the FEM solver (TRIDENT) and the blade mesh is deformed.
- The deformed mesh is used to perform the fluid analysis for the second iteration.
- The whole process is repeated until the difference of the thrust between two consecutive steps is zero and blade deflection has reached the equilibrium.

5.4 Case 4: RANS-FEM Implicit Two-Way Coupled FSI Analysis with STAR-CCM+

In this analysis case, the complete FSI analysis is done by using STAR-CCM+. The structural solver used in this case is the one integrated in STAR-CCM+. The fluid and structural calculations are done in the same software without any human intervention, therefore, it is characterised as strong two-way coupled FSI analysis and the results obtained are considered to be the most accurate.

The main characteristics of all of the cases are summarized in the Table7 below:

Table 7: Summary of all the isotropic blade cases

ISOTROPIC BLADE CASE					
		Case1	Case2	Case3	Case4
Fluid solver		PROCAL	STAR-CCM+	PROCAL	STAR-CCM+
Fluid analysis type		Steady	Steady	Steady	Steady
FEM	Solver	NASTRAN	NASTRAN	VAST	STAR-CCM+
	Pre post processor	FEMAP	FEMAP	TRIDENT	STAR-CCM+
FEM analysis type		Linear Static	Linear static	Non-linear static	Non-linear dynamic
Coupling type		One-way	One-way	Explicit two-way	Implicit two-way

5.5 Comparison

5.5.1 Input Comparison

Before comparing the obtained results from different approaches, it is important to compare the inputs.

- The mesh used in the first case is similar to the third case. It is done by importing the model generated for ComPropApp in FEMAP. It is important to mention that ComPropApp can only support structured mesh which cannot be generated in FEMAP due to complex geometry, therefore, the FEMAP model cannot be imported in ComPropApp. As both software have the same model, hence, the differences in the results are solely due to the solvers and FSI techniques used to perform the analysis. The blade is discretized by 50 x 50 (50 elements chordwise and 50 in the radial direction) parabolic hexahedral elements. There is only one element in the blade thickness. The mesh used in the first case is shown in the Fig.25.

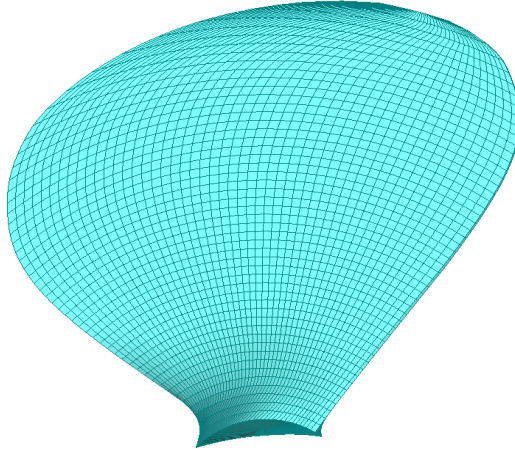
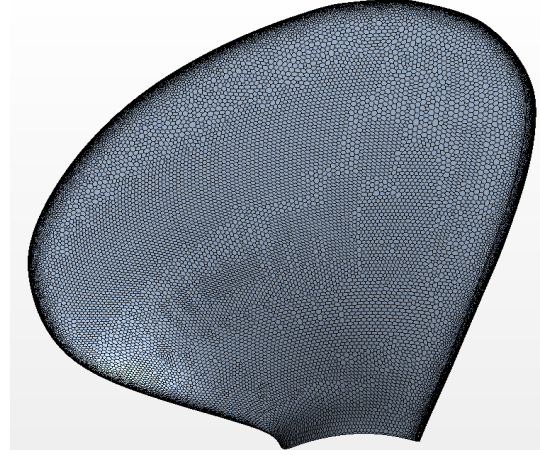


Figure 25: Mesh used in case 1

- In the second case, different meshes are used for the structure and the fluid solver. In case of the fluid solver, a very fine polyhedral mesh is generated to capture the fine details of the model which is essential for the CFD calculations. In case of the FEM solver, the finer mesh than the first case is used in FEMAP. It has 100 x 100 elements (100 elements chordwise and 100 elements in radial direction). It is done to minimize the discrepancies that can rise during the mapping of pressure and to have a better comparison. Although the FEM mesh is finer than the other cases, the results should not be affected much as the difference of the results is found to be less than 1% through mesh convergence study done in section 3.3. Both structural and fluid meshes are shown in the Fig.26a and Fig.26b, respectively.



(a) Mesh for the FEM solver (FEMAP)



(b) Mesh for the fluid solver (STAR-CCM+)

Figure 26: Mesh used in case 2

- The mesh used in ComPropApp is shown in the Fig.27. The blade is discretized by 50 x 50 (50 elements chordwise and 50 in radial direction) parabolic hexahedral elements. There is only one element in the blade thickness, it can't be increased due to the software limitations. The same mesh is used by the fluid and structural solvers of ComPropApp.

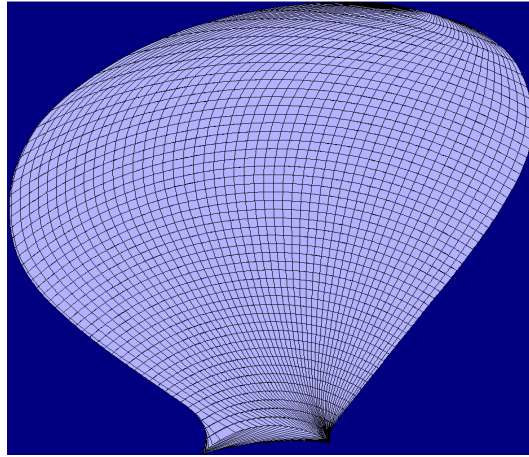


Figure 27: Mesh used in case 3 (ComPropApp)

- The mesh used in the fourth case is generated by superimposing the fluid and structure meshes. The fluid mesh has fine polyhedral elements while the structural mesh has coarse linear tetrahedral elements. The structure mesh is refined at the blade edges to have better approximation of the curvature. There are four elements in the blade thickness for the FEM mesh. The both meshes can be seen in the Fig.28. The coarse tetrahedral mesh on the blade's surface is the FEM mesh while

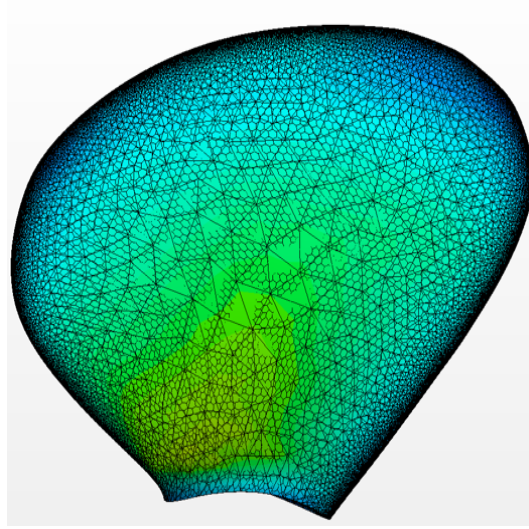


Figure 28: Mesh used in case 4 (STAR-CCM+)

the fine polyhedral mesh in the background of tetrahedral mesh is the fluid mesh.

The mesh characteristics for the different cases are summarized in the table below:

Table 8: Isotropic blade case: Mesh comparison

	Case 1	Case 2	Case 3	Case 4
Mesh type (fluid solver)	Quads	Polyhedral	Quads	Polyhedral
Mesh type (FEM solver)	Hexahedral	Hexahedral	Hexahedral	Tetrahedral
Elements no. in thickness	1	1	1	4
Total elements (FEM solver)	2500	10000	2500	246144
Total elements (Fluid solver)	2500	9 million	2500	9 million

5.5.2 *Output Comparison*

In this section, the results obtained are compared and discussed.

- The maximum blade nodal deflection and maximum Von Mises stress obtained in the first case are shown in the Fig.29. The maximum deflection will be at the tip of the blade and maximum stresses at the root of the blade because it is like a cantilever beam case.

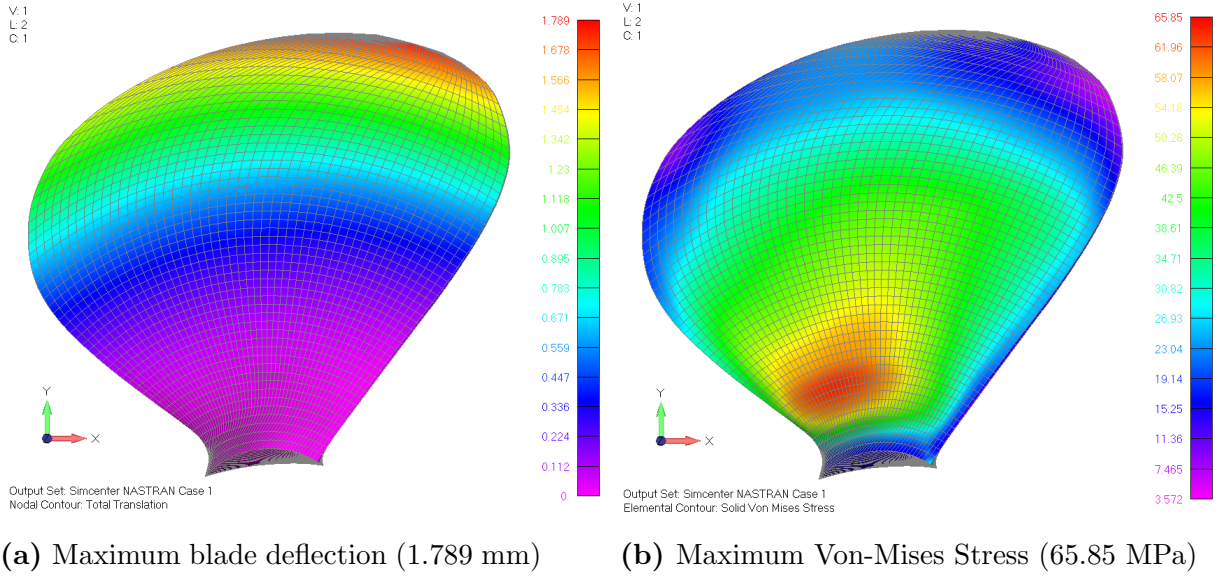


Figure 29: Results obtained in case 1

- The maximum blade deflection and maximum Von Mises stress obtained in the second case are shown in the Fig.30.

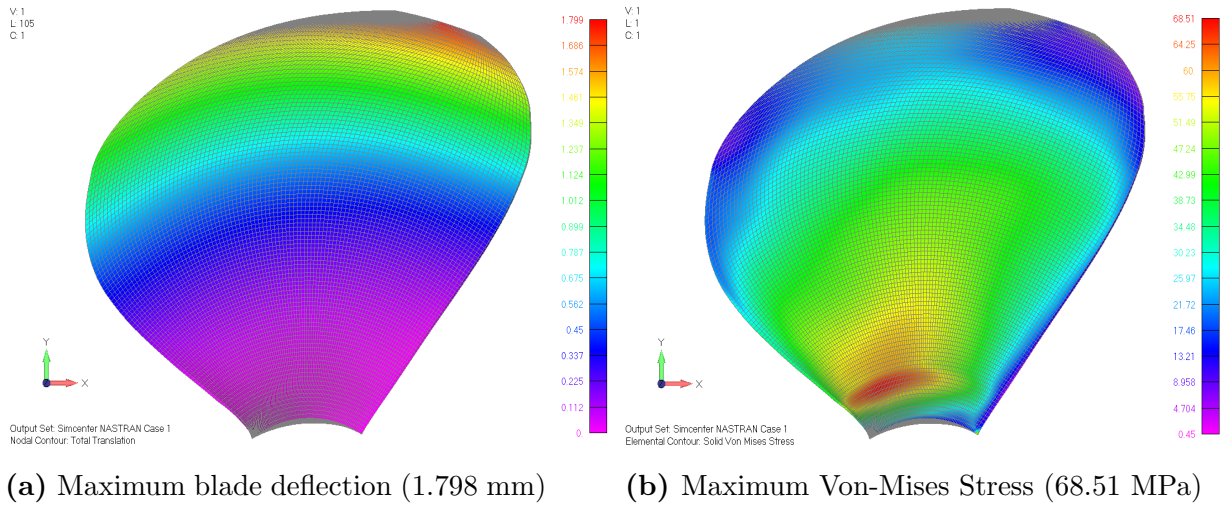


Figure 30: Results obtained in case 2

- The maximum blade deflection obtained in the third is shown in the Fig.31. The contour distribution of the Von Mises stress is not possible to show with ComProApp as this feature of the software still needs improvement. The value for the maximum Von Mises stress is taken from the output files generated by TRIDENT and it is tabulated in the Table.9 for the output comparison.

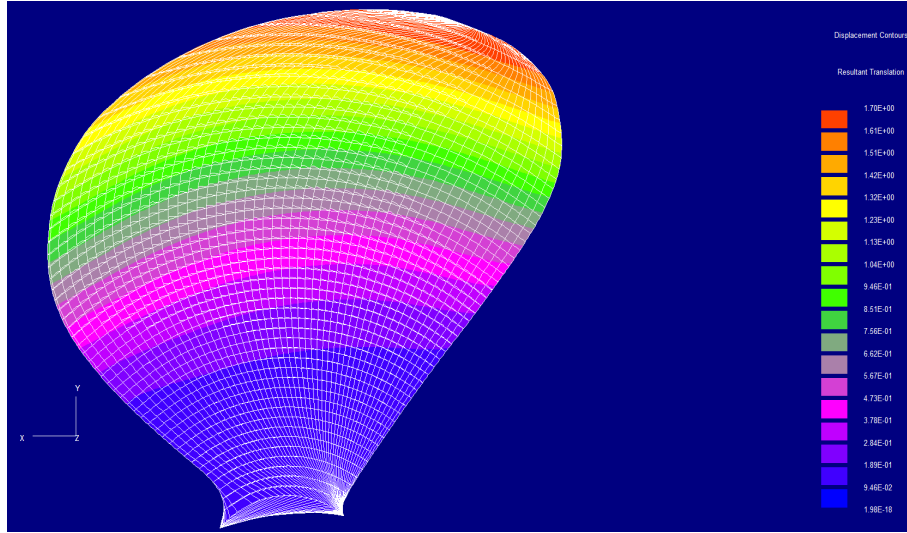
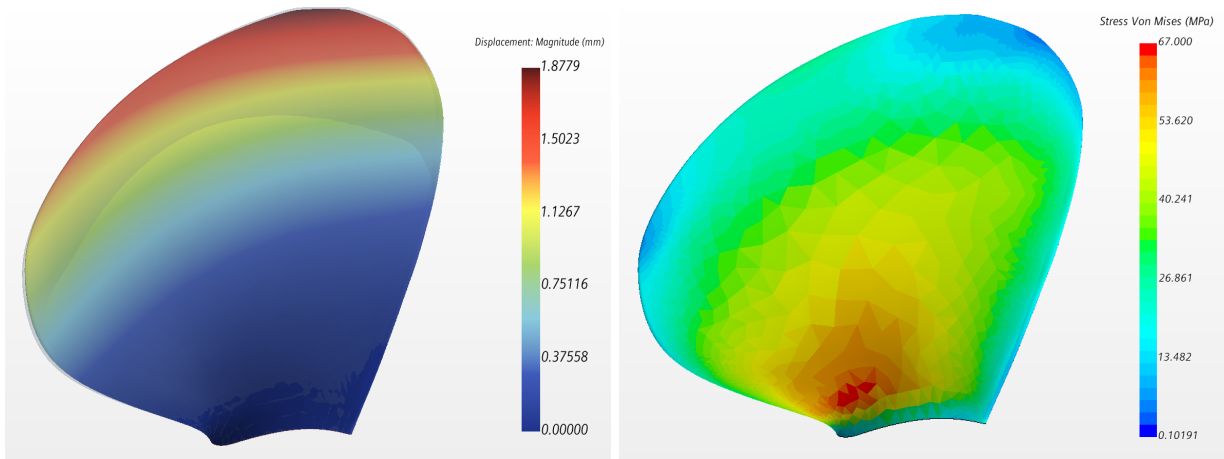


Figure 31: Maximum displacement for case 3 (1.70 mm)

- The maximum blade deflection and maximum Von Mises stress obtained in the fourth case are shown in the Fig.32.



(a) Maximum blade deflection (1.87 mm)

(b) Maximum Von-Mises Stress (66.5 MPa)

Figure 32: Results obtained in case 4

The output of all the cases are tabulated in the Table.9 and the results are compared with the third case (FSI analysis by ComPropApp).

Table 9: Isotropic blade case: Output comparison with complete FSI in ComPropApp

					Relative difference	
	Case 1	Case 2	Case 3	Case 4	Case 1 and Case 2	Case 3 and Case 4
T=Thrust (N)	50720	49195	50160	49420	3.10%	1.50%
Q=Torque (N.m)	10673	10220	10372.51	10280	4.43%	0.90%
Max. Displacement (mm)	1.789	1.798	1.7	1.875	-0.5%	-9.33%
Max. Von Mises stress (MPa)	65.85	68.51	65.7	66.5	-3.88%	-1.20%

The comparison and critical analysis of the results is as follows:

- To check the effect of the linear static analysis and non-linear static analysis, the FEM model and loads generated in third case are imported and solved FEMAP by using linear static analysis. It is found that the relative difference between the displacement and Von Mises stress is 0.41% and -1.22%. Therefore, it is found that the type of analysis affects the results. This analysis is performed because of the following two reasons:
 1. To compare the results of the linear and non-linear static analysis because for the composite blade it is not possible to perform non-linear analysis by using FEMAP. Therefore, this comparison can be used as the benchmark model for the future analysis.
 2. FEMAP is a commercial software which has advanced features to deal with the composites, whereas the FEM solver of the ComPropApp (TRIDENT) has many limitations as it is in the developing phase for composite material analysis. Therefore, it is required to validate the results of the model generated by ComPropApp but solved in FEMAP.
- It can be noticed that the thrust calculated by ComPropApp is roughly 1.5% to 3% more than STAR-CCM+ value. One of the potential reason could be the viscous effects which are neglected by ComPropApp as it is a BEM solver. it is also confirmed by the software's developer that no viscous correction is made in the current version of the software (Wijngaarden, Personal conversation). Similar kind of difference is observed by the researchers (Maljaars et al. (2018)) when the thrust obtained from BEM and RANS analysis of a marine propeller are compared.
- The comparison of the first case (BEM-FEM one-way coupled FSI) and the second

case (RANS-FEM one-way coupled FSI) shows the relative difference of 3.1% to 4.43% for the thrust and torque values while an unexpected trend is noticed for the blade displacement. The second case has 3.1% less thrust but 0.5% more deflection. To investigate the reason of this anomaly, several factors like resultant moments and forces are compared. At first, it is expected that the second case might have more resultant moment which could be the reason of large deflection, but the comparison shows that the first case has higher moment and still it gives less nodal deflection.

Table 10: Comparison of the moments at blade root

	$M_{root}(KN.m)$
Case 1	2916.41
Case 2	2512.63
Relative difference	16.07%

Therefore, the reason of anomaly could not be found by the comparison of the moments. The distribution of pressure field is very important for the deflection, therefore, a comparison is done for the pressure distribution at the pressure and suction side of the blade. Apparently, the pressure distribution on the pressure side of the first case seems higher than the pressure side of the second case which seems to be inline with the results that the thrust generated by the BEM solver is more than the RANS solver. The pressure distribution of the suction side of the first case shows that in the case BEM solver, the pressure distribution on the suction side is negative only at the small area close to the edge and positive everywhere else while in the second case the suction side has larger area with negative pressure distribution. The visual observation gives a notion that the reason for the higher deflection in the second case is might be due to this difference in the pressure distribution. The pressure distribution comparison on the pressure side of the blade for the first two cases is shown in the Fig33.

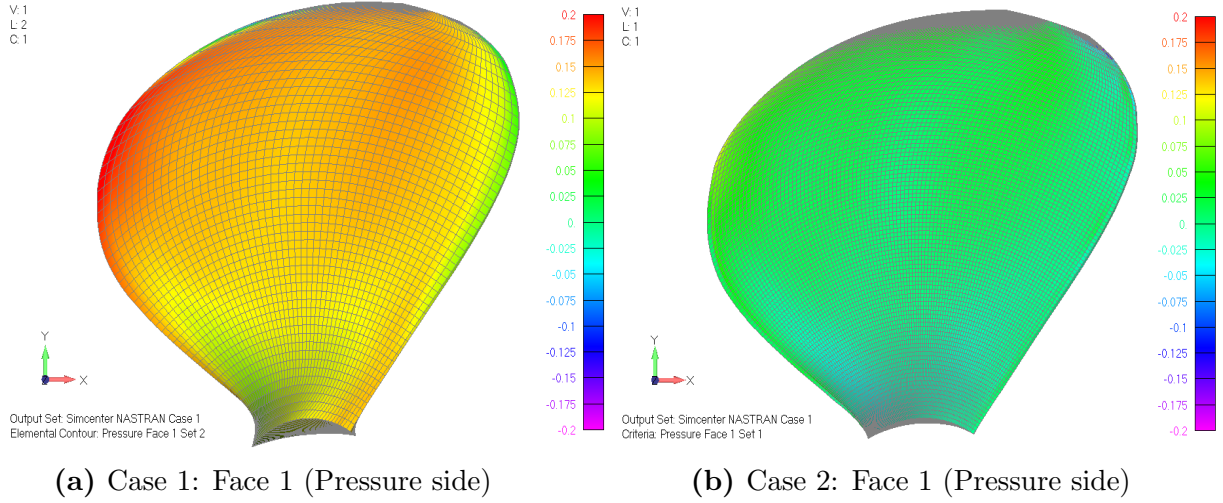


Figure 33: Comparison of the pressure side pressure

The pressure distribution comparison on the suction side of the blade for the first two cases is shown in the Fig34.

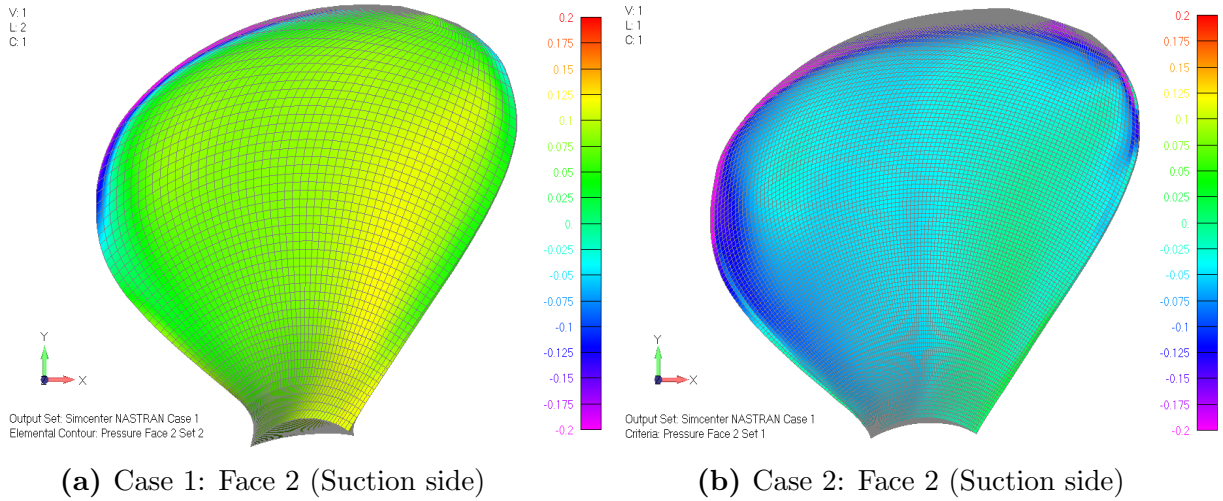


Figure 34: Comparison of the suction side pressure

To confirm the observation further analysis is performed by plotting the pressure difference distribution against the chord length for the two different radial sections of the blade. The first radial section is selected at the middle of the blade. The pressure difference at the middle radial section is found to be exactly same for the BEM and RANS solver. In the Fig33 and Fig.34, the pressure plots for the two solvers look different because the BEM solver is including static pressure. The distribution of pressure difference between the pressure and the suction side for the

mid radial section of the blade is plotted against the normalised chord length which is shown in the Fig36.

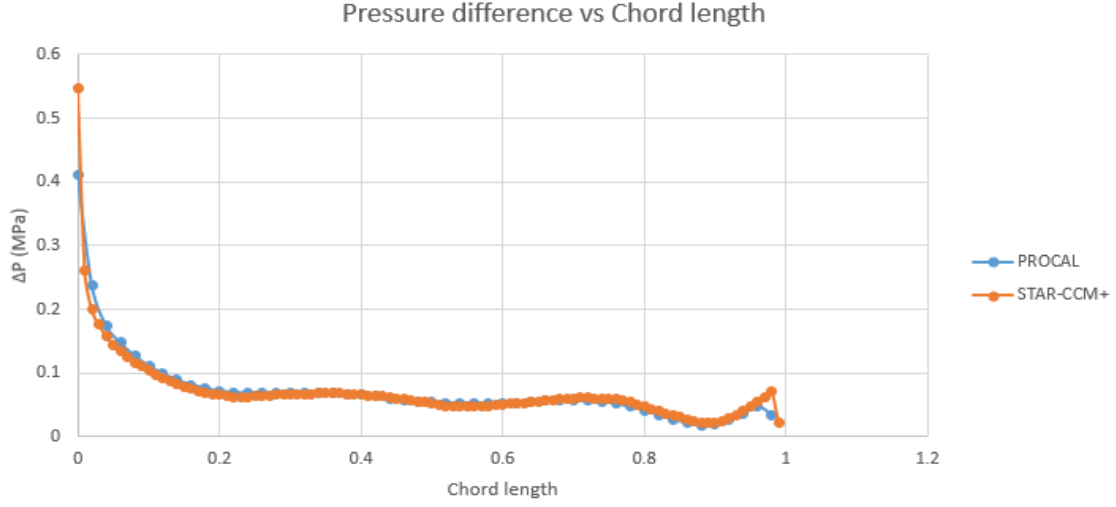


Figure 35: Pressure difference at the middle of the blade

The pressure difference plots at the mid radial section were unable to describe the reason of the anomaly, therefore, the pressure distribution was plotted at the tip of the blade. The pressure difference at the tip was found to be different for BEM and RANS solvers. The pressure difference values in the case of RANS solver are higher than the values obtained in the case of BEM solver. Therefore, this could be one of the reasons of having higher blade deflection for the RANS solver case even though the thrust is slightly lower than the BEM solver.

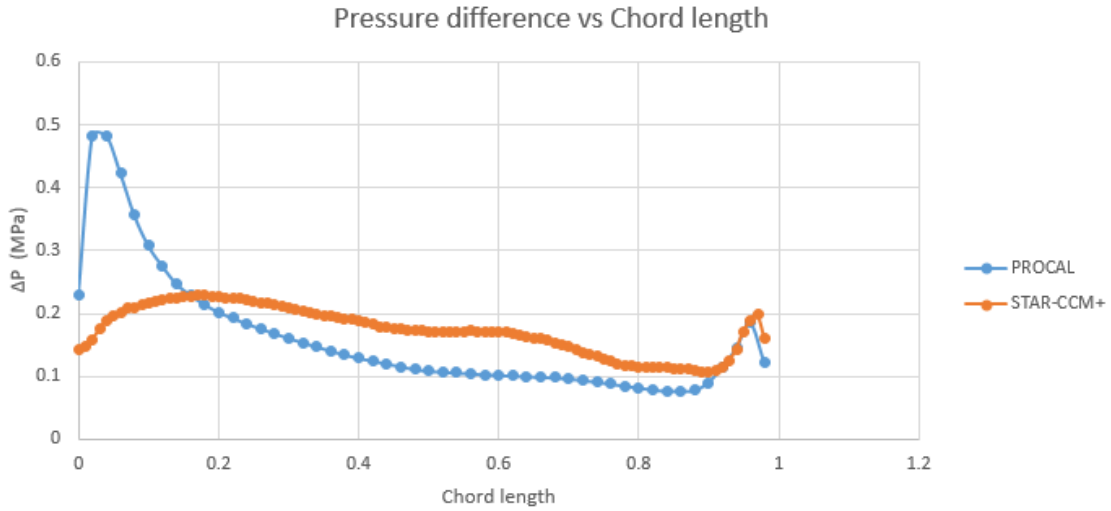


Figure 36: Pressure difference at the tip of the blade

This shows that no tip pressure correction is applied in the ComPropApp as it is very important to get the realistic deflection of the blade. Maljaars et al. (2017a) performed the analysis by using PROCAL and stated that the tip pressure correction is significant for the blade deflection. In fact, it is confirmed by the developer of ComPropApp that no tip pressure correction is applied at the moment and it will be used in the future versions of ComPropApp (Wijngaarden, Personal communication).

- On the contrary, the comparison of complete FSI analysis by ComPropApp with RANS-FEM strongly two-way coupled FSI analysis shows that the relative difference in thrust is 1.5% while it is -9.33% for the blade deflection. It means STAR-CCM+ generated less thrust but yielded in more blade deflection. In addition to the fact, that BEM solver has lower pressure difference at the blade tip than the RANS solver the discrepancy can be justified by the fact that the FEM models used in two cases are very different. In the case of ComPropApp, there is a structured hexahedral mesh model with only one element in blade thickness while in STAR-CCM+ there is a tetrahedral mesh model with four elements in thickness. A benchmark study (Annex 1), is done to study the effect of hexahedral and tetrahedral mesh on blade deflection and a difference of about 1.5% to 3.5% is found. Another factor is the type of analysis carried out in both cases is different i.e. non-linear static analysis in case of ComPropApp and non-linear dynamic analysis in the other case.
- The comparison of computational time and power is an important factor to decide the suitable method for the simulation. The comparison of computation time and power for case three and case four is shown in the Table.11.

Table 11: Comparison of computation time for BEM and RANS FSI Analysis

Event		Case 3	Case 4
Fluid Simulation Time	Pre processing	20 mins	5 days
	Computation	30 mins	3 day
	Post Processing	10 mins	2 hours
	Total time	60 mins	8 days
CPU specifications	Processor	Intel i7	Intel i7
	Number of cores	4 cores	4 cores
	RAM	16 GB	16 GB

It is clear from the comparison that the time and computation power taken by the RANS solver is significantly higher than the BEM solver. Moreover, in the present case, the steady fluid analysis is carried out which is less intensive in terms of computation time and power as compare to unsteady case. For unsteady case the RANS computation can take several days.

6 COMPOSITE BLADE CASE

The FSI analysis done by using composite blade is divided into four cases depending on the type of the solver and FSI method. The flow chart shown below in Fig.37 shows the different analyses performed for this case.

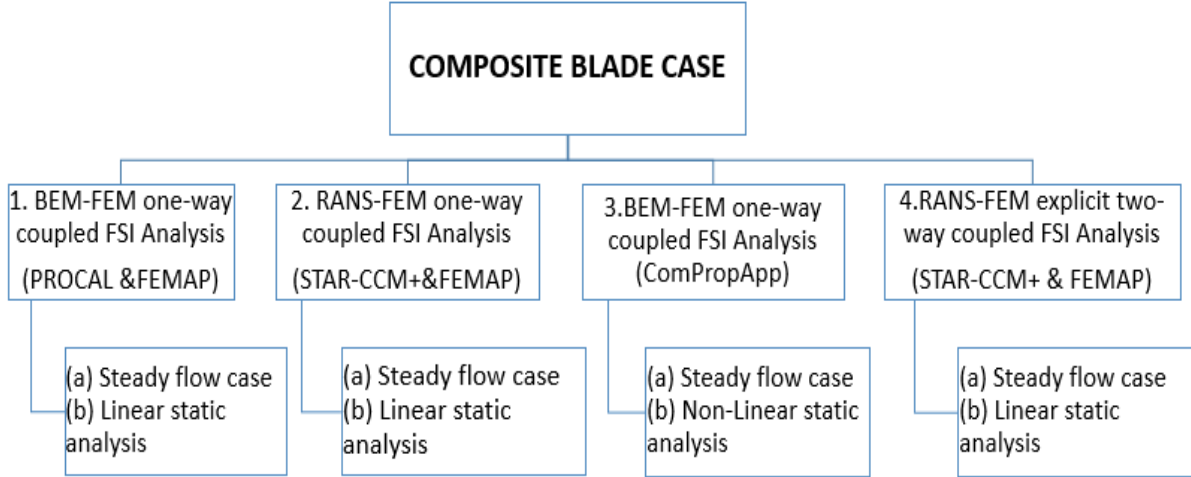


Figure 37: Analysis performed for the composite blade case

6.1 Case 1: BEM-FEM One-Way Coupled FSI Analysis

In the first case, the FSI analysis is performed by one one-way coupling of the BEM and FEM solvers. The characteristics of this analysis are as follow:

- The fluid loads are generated by steady flow analysis in BEM solver (PROCAL).
- The fluid loads are imported in FEMAP and linear static analysis is performed.

6.2 Case 2: RANS-FEM One-Way Coupled FSI Analysis

In the second case, the FSI analysis is done by one-way coupling of the RANS and FEM solvers. The characteristics of this analysis are as follow:

- The fluid loads are generated by performing steady flow analysis in RANS solver (STAR-CCM+).
- The fluid loads are imported in the FEM solver (FEMAP) and static linear analysis is performed.

6.3 Case 3: BEM-FEM One-Way Coupled FSI Analysis with ComPropApp

In the third case, the FSI analysis is performed completely in ComPropApp, due to some technical issues the analysis could be performed only for the first iteration. Hence, it is only the first iteration of the explicit two-way coupled FSI analysis. Following are the steps performed by ComPropApp to perform this analysis:

- The BEM fluid solver (PROCAL) performed analysis and fluid loads are generated.
- ComPropApp's interface is used to transfer the fluid loads to structural model mesh and non-linear static analysis is performed in TRIDENT.

6.4 Case 4: RANS-FEM Explicit Two-Way Coupled FSI Analysis with STAR-CCM+ and FEMAP

In the fourth case, the FSI Analysis is performed two-way coupling of the RANS and FEM solvers. Such kind of analysis is performed when the displacement or deformation of the geometry due to fluid loads is large enough to change the hydrodynamics. Following are the steps performed in this analysis:

- In the first step, the CFD analysis is carried out in the RANS solver (STAR-CCM+) and fluid loads are generated.
- In the second step, the fluid loads are mapped and then imported in FEM solver (FEMAP) and linear static FEM analysis is performed.
- In the third step, the calculated geometry's displacement is imported into the fluid solver (STAR-CCM+) and the mesh is morphed to take into account the new displaced geometry for the fluid analysis.
- The new fluid loads are generated for the displaced geometry and the whole process is repeated until the equilibrium is reached.

This process required six iterations to reach the equilibrium position for blade displacement. The convergence is shown in the Fig.38.

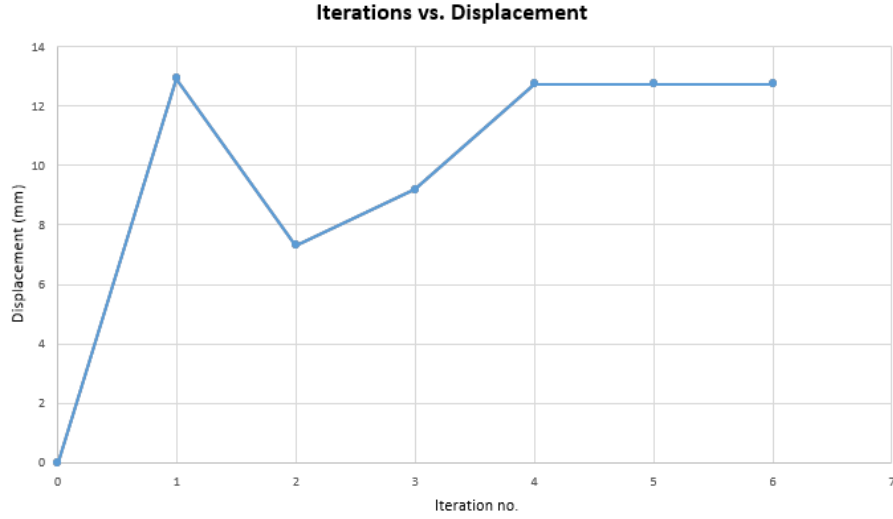


Figure 38: Convergence graph of blade displacement

The main characteristics of all of the cases are summarized in the Table.12 below:

Table 12: Summary of all the cases

COMPOSITE BLADE CASE					
		Case1	Case2	Case3	Case4
Fluid solver		PROCAL	STAR-CCM+	PROCAL	STAR-CCM+
Fluid analysis type		Steady	Steady	Steady	Steady
FEM	Solver	NASTRAN	NASTRAN	VAST	NASTRAN
	Pre post processor	FEMAP	FEMAP	TRIDENT	FEMAP
FEM analysis type		Linear Static	Linear static	Non-linear static	Linear static
Coupling type		One-way	One-way	One way	Explicit two-way

6.5 Comparison

The mesh generation and definition of laminates properties is a laborious job which is done by creating the .CDR and .PRP files. These files are required by ComPropApp to perform analysis for the composite blade case. In .PRP file the properties of laminates, layup sequence and direction of different layers are defined, whereas, in .CDR file the discretization of blade geometry and material/laminate mapping corresponding to the elements are defined.

6.5.1 Input Comparison

To avoid the discrepancies in the FEM models, the same mesh is used in ComPropApp and FEMAP. It is done by importing the mesh generated for ComPropApp in FEMAP. It is important to mention that unlike the isotropic case, ComPropApp was unable to import the material properties correctly in FEMAP. Therefore, only the mesh was imported in FEMAP while the layup description and material orientation were separately done. The material orientation done in FEMAP is according to the study performed by Maljaars et al. (2017b). It is observed that the way material orientation is defined in FEM solver can significantly affect the FEM results. As such, the model in FEMAP could be slightly different than ComPropApp. The FEM mesh is shown the Fig.39.

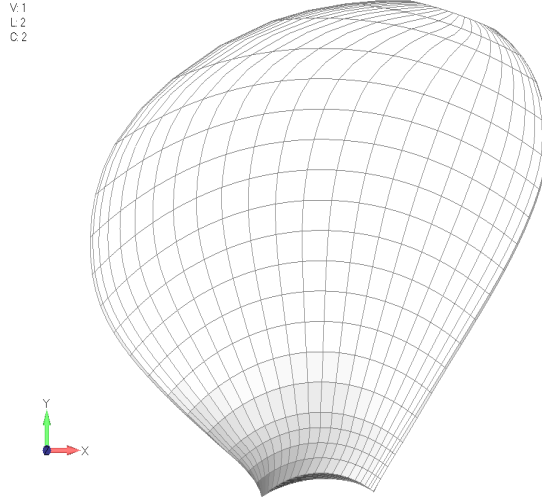


Figure 39: FEM mesh used for composite blade

The mesh characteristics for the different cases are summarized in the Table13:

Table 13: Composite blade case: Mesh comparison

	Case 1	Case 2	Case 3	Case 4
Mesh type (fluid solver)	Quads	Polyhedral	Quads	Polyhedral
Mesh type (FEM solver)	Hexahedral	Hexahedral	Hexahedral	Hexahedral
Elements no. in thickness	1	1	1	1
Total elements (FEM solver)	437	437	437	437
Total elements (Fluid solver)	437	9 million	437	9 million

An important point to mention is that in the case of composite blade there is a discrepancy

of 0.45% in the diameter of propeller used in ComPropApp and STAR-CCM+. The diameter of the propeller used in STAR-CCM+ is 0.45% bigger than the one used in ComPropApp due to which there is a discrepancy in the values of thrust and torque. The effect of this on the output results is discussed in detail in the next section of the report.

6.5.2 Output Comparison

The comparison of the results are presented as follow:

- In the first case, results obtained for the maximum blade deflection, maximum X normal stress among all layers (shown on the top surface), maximum Y normal stress among all layers (shown on the top surface) and maximum XY shear stress among all layers (shown on the top surface) are shown in the Fig.40.

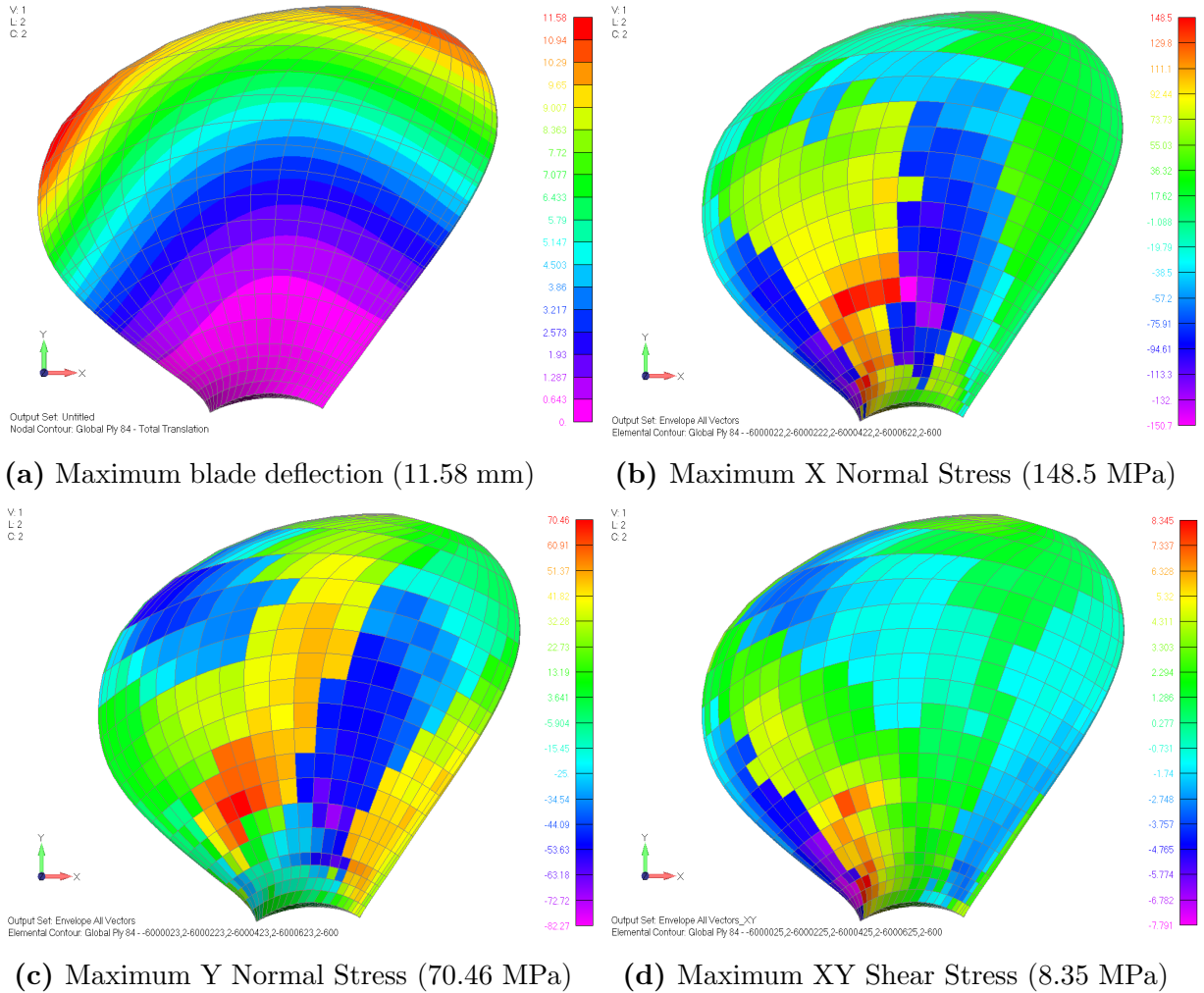


Figure 40: Results obtained in case 1

In the Fig.40, the positive values correspond to tension while the negative values correspond to compression.

- The results obtained for the maximum blade deflection, maximum X normal stress for all layers projected on the top surface, maximum Y normal stress for all layers projected on the top surface and maximum XY shear stress for all layers projected on the top surface in case two are shown in the Fig.41.

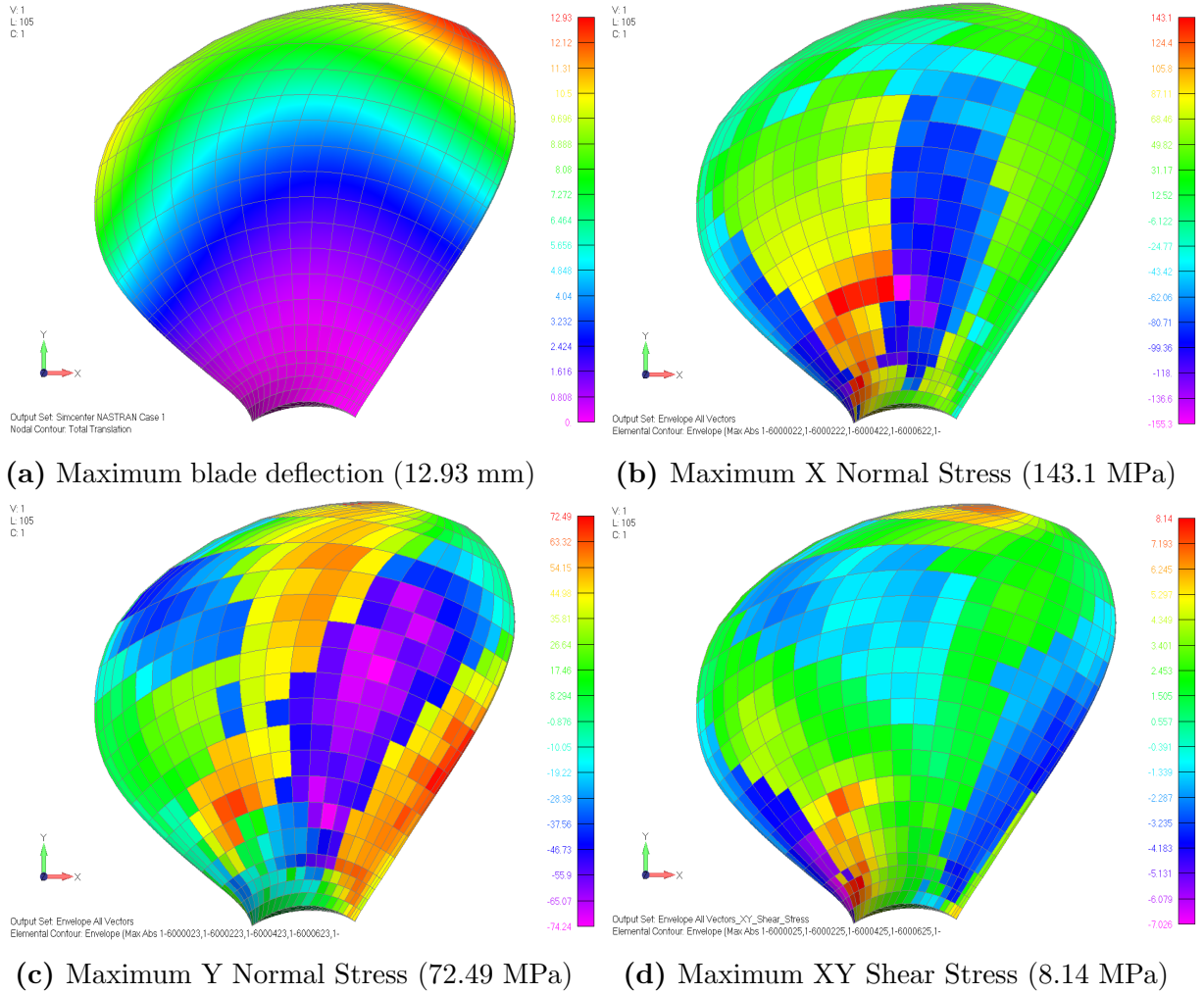


Figure 41: Results obtained in case 2

- The value of maximum displacement obtained in case 3 is shown in the Fig42. The values of maximum X, Y and XY stress could not be obtained due to the limitation of ComPropApp as it is unable to show the ply-by-ply stresses. The feature is still under process and expected to be available in the future.
- The results obtained for the maximum blade deflection, maximum X normal stress for all layers projected on the top surface, maximum Y normal stress for all layers

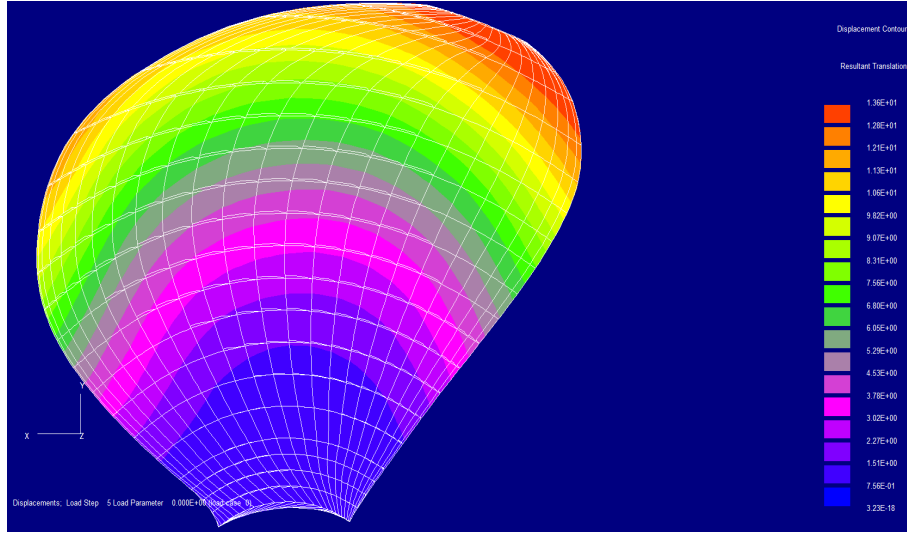


Figure 42: Maximum displacement for case 3 (13.6 mm)

projected on the top surface and maximum XY shear stress for all layers projected on the top surface in case four are shown in the Fig.43.

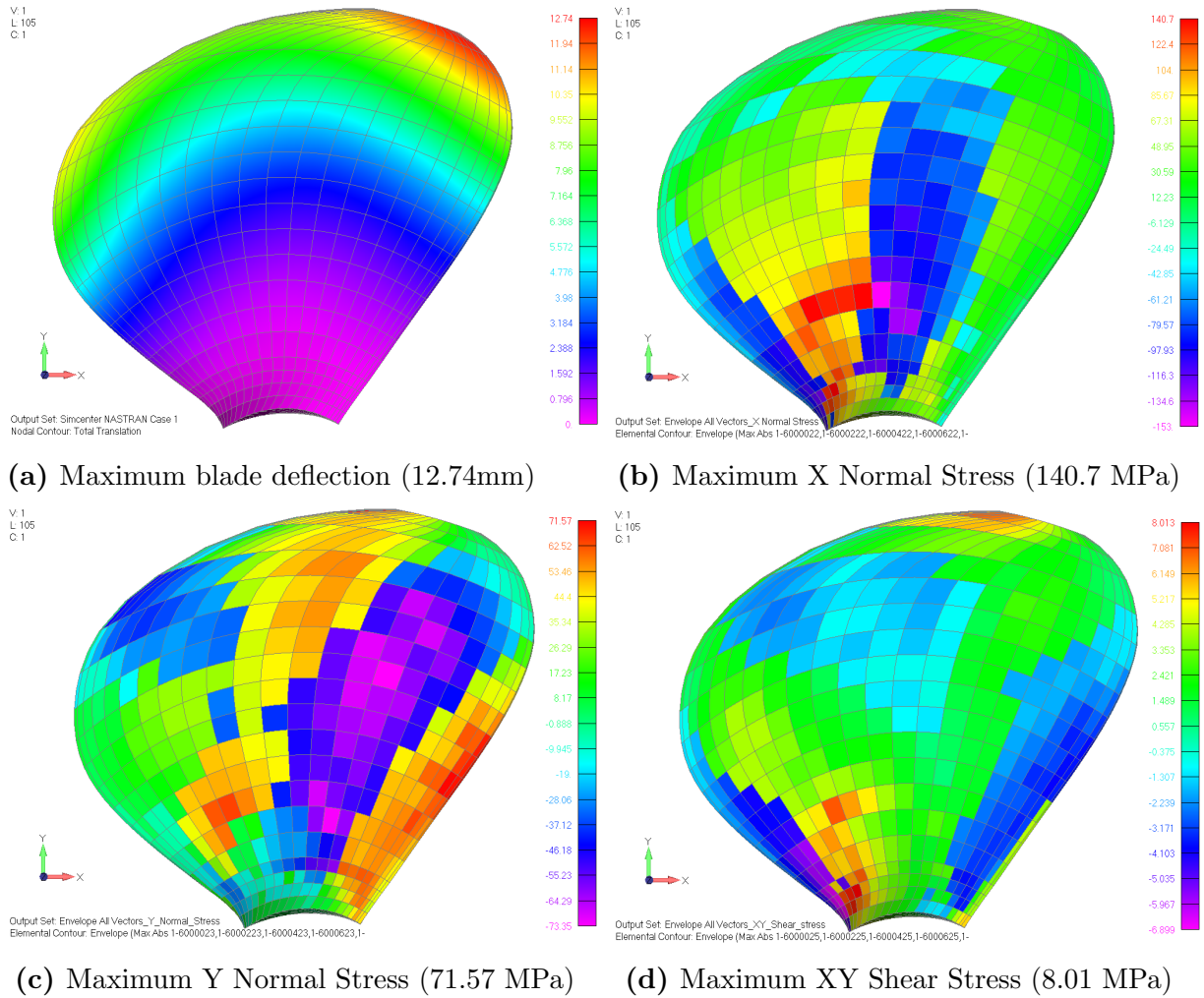


Figure 43: Results obtained in case 4

In the Fig.43, the positive values correspond to tension while the negative values correspond to compression. The results of all the cases are tabulated in the Table14 below:

Table 14: Composite blade case: Output comparison with FSI in ComPropApp

	Obtained Values				Relative difference with Case 3		
	Case 1	Case 2	Case 3	Case 4	Case 1	Case 2	Case 4
T=Thrust (N)	48671.55	49195	48671.55	48456.6	0.00 %	1.08 %	-0.44%
Q=Torque (N.m)	10313.35	10220	10313.35	10099.5	0.00 %	-0.91 %	-2.07%
Max. Displacement (mm)	11.58	12.93	13.6	12.74	-14.85 %	-4.93 %	-6.32%

The comparison and critical analysis of the results is as follows:

- It can be noticed that the blade tip displacement is very large as compared to the thickness of the tip. Hence, this is classified as the large displacement case and geometrical non-linear effects become significant to correctly define the FEM results i.e. the displacement and the stresses.
- It can be noticed that the thrust generated in the second case (RANS-FEM one-way coupled FSI) is more than the third case (FSI analysis by ComPropApp), whereas, in the current version of ComPropApp there is no viscous correction is applied, therefore, it should be inline with the study done by Maljaars et al. (2017a) in which BEM solver generated higher thrust than the RANS solver. The reason for this discrepancy is the slight variation in the propeller diameter which is already mentioned in the input comparison section of the report. The diameter of the propeller used in STAR-CCM+ is 0.45% bigger than the one used in ComPropApp. The effect of diameter on the thrust is significant which can be noticed from Eq.2. This discrepancy is also contributing to the relative difference obtained in by the comparison of the case three and case four.
- The blade deflection comparison of the first case and the second case shows a relative difference of 14.85% while there is a relative difference of 6.32% for blade displacement between the third and the fourth case. Despite the differences due to linear static FEM analysis and nonlinear static FEM analysis done by the two FEM solvers used in the third and fourth case, there are some other factors. Unlike the isotropic case, ComPropApp is unable to import the material properties correctly in FEMAP. Therefore, only the mesh, ply layup and material properties are exported

while the material orientation is separately done in FEMAP. The CRS team is working to introduce a better interface between ComPropApp and FEMAP.

The FSI analysis carried out in fourth case is explicit two-way coupled in which pressure field and geometry displacement is taken from one software to another software several times. This caused the loss of pressure and displacement fields. The loss of pressure and displacement field during the importing and mapping process is summarized in the Table15.

Table 15: Relative difference of imported and mapped Pressure and displacement fields

	% loss actual vs. mapped disp	% loss actual vs mapped LE pressure
1	-0.008	-59.221
2	-0.104	-67.6004
3	-1.989	-2.557
4	-0.008	-21.014
5	-0.008	-21.0176

The second column shows the percentage of displacement lost during the mapping of displacement from the coarse structural mesh to the fine CFD mesh. The process of mapping of displacement is carried out in the STAR-CCM+ and it also does some approximation because of the huge difference in the mesh sizes. It can be noticed that the loss of displacement during each stage is low but if all the steps are taken into account then it can contribute to a small percentage of the discrepancy. The difference between the imported verses the mapped displacement field for one of the iteration steps of the analysis is shown in the Fig.44.

The third column shows the percentage of pressure loss (comparison of maximum values), especially at the leading edge, during the mapping process. In case of the pressure, a large percentage difference is noticed. The reason of large pressure loss during the process of pressure mapping from the fluid mesh to the FEM mesh is the coarse FEM mesh which causes poor description of the geometry. In fact, it is not completely matching the fluid blade at the upper tip, leading and trailing edges where the pressure is maximum. The explanation of the fact that despite such large pressure variation the final result has only 6% difference of blade deflection with the third case (FSI in ComPropApp) can be understood from the Fig.45.

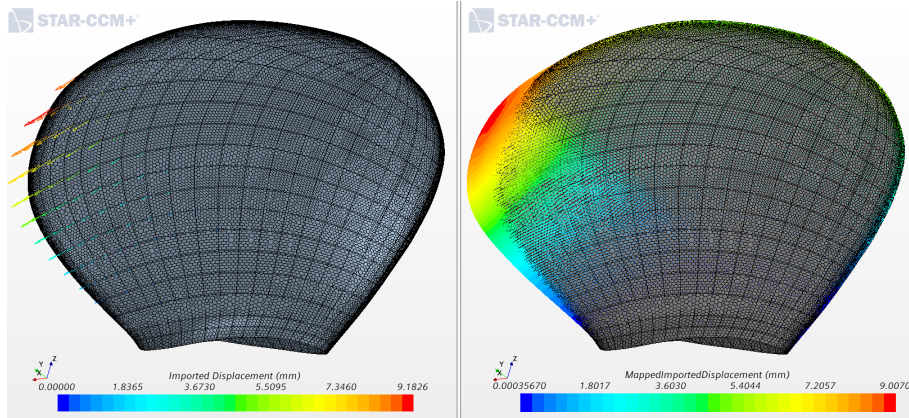
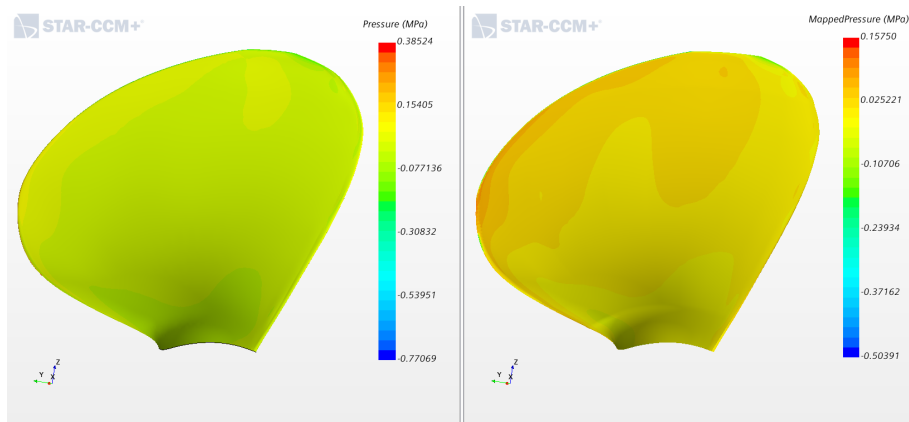
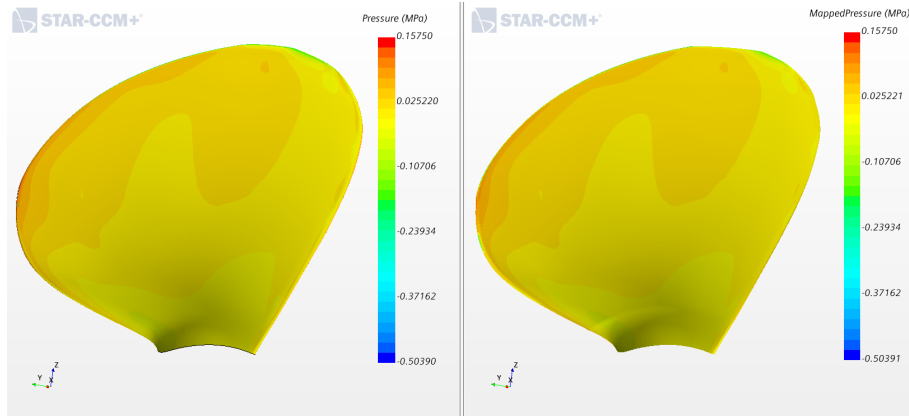


Figure 44: Imported vs. mapped displacement field



(a) Actual Pressure distributions



(b) Pressure distribution with same legend

Figure 45: Actual vs. mapped pressure field

It can be noticed in the Fig.45(a) that maximum calculated pressure value is shown as 0.385 MPa whereas most of the blade surface shows the pressure between -0.3 to 0.15 MPa. The highest pressure exists on the small part of the leading edge. In Fig.45(b), it can be seen that the actual and mapped pressure fields are almost

the same when same legends are used. Therefore, it can be concluded that missing the high pressure at trailing edge will not have significant effect. In unsteady flow conditions and dynamic analysis, such effects might be significant, therefore, it is considered important to discuss them.

- The comparison of the computation time and power for the third and the fourth case are shown in the Table16.

Table 16: Comparison of computation time for BEM and RANS FSI Analysis

Event		Case 3	Case 4
Fluid Simulation Time	Pre processing	4 hours	5 days
	Computation	30 mins	6 hours
	Post Processing	10 mins	10 hours
	Total time	5 hours	5.5 days
CPU specifications	Processor	Intel i7	Linux Cluster
	Number of cores	4 cores	112 cores
	RAM	16 GB	60 GB

Just like isotropic blade case, the time taken by STAR-CCM+ is significantly higher than the ComPropApp.

7 CONCLUSION

The study is divided into two cases, first case is for the FSI analysis of isotropic blade and the second one is for the FSI analysis of composite blade. Each of these cases are further divided into four sub cases depending on the type of fluid solvers, i.e. BEM and RANS solvers, and the type of FSI coupling, such as one-way and two-way coupled FSI analysis.

In the isotropic blade case, the comparison of the explicit two-way coupled FSI analysis by ComPropApp with the implicit two-way coupled FSI analysis performed by STAR-CCM+ shows that the relative difference of the thrust and torque quite small about 1% to 1.5% while the difference for the blade deflection is about 9.5% which can be reduced if the blade tip pressure correction is applied in ComPropApp. On the other hand, the computation time and power spent for the analysis in STAR-CCM+ is significantly higher than the ComPropApp.

In the case of the composite blade, the comparison of the results obtained from ComPropApp with the explicit two-way coupled FSI analysis performed by STAR-CCM+ and FEMAP shows the relative difference of 6.3% for blade deflection and 0.5% to 2% for the thrust and torque. The reason for having this discrepancy is due to the fact that the two FEM models used in ComPropApp and FEMAP are not exactly the same and the blade tip pressure correction is not applied in the current version of ComPropApp. Therefore, these factors contributed to the discrepancies in the results. The development of ComPropApp is still under process and such shortcomings will be eliminated in the future versions. Like isotropic case, ComPropApp took less than an hour to do the computation, whereas, STAR-CCM+ took several days.

Although, the relative difference of results for both cases is in the acceptable range, there are some essential improvements that should be done in ComPropApp before it can be used for the design evaluation of composite propellers.

It is the first time, when ComPropApp is used for an industrial application, therefore, the task was quite challenging. The complex geometry of FabHeli pushed ComPropApp beyond its limits and helped to identified the improvements that can make it an ideal tool for design evaluation. The classification society considers ComPropApp as a promising tool that would be able to speed up the design evaluation process. The tool can also be useful for the designers. It enables the designers to test several configurations of the

propellers as it is much faster and cheaper than the conventional RANSE solvers. However, this study is done in steady flow condition for only one advance coefficient which is about 0.7 and further investigation should to be done for other values of advance coefficients. In the future, the improvements will be implemented in the ComPropApp and further investigation will be done for the unsteady fluid analysis and the wider range of advance coefficients.

ACKNOWLEDGEMENTS

On the very outset of this report, I would like to thank all the personages who have helped me in this endeavor. I would not have made headway in the project without their active guidance, help, encouragement and cooperation.

I am extremely thankful and pay my gratitude to my tutor **Mr. Stephane PABOEUF** and my seniors **Mr. Joseph Praful TOMY**, **Mr. Benjamin COLLIER** and **Mr. Luc MOUTON** from Bureau Veritas M&O Composite Materials section of Expertise Department, for their valuable guidance and support for the structural aspect of the project.

I extend my gratitude to **Mr. Alexandre HERTOUT** from Siemens and **Mr. Sébastien LOUBEYRE**, **Mr. Loïc MAZAS** and **Mr. Corentin DOBRAL** from BV Solutions M&O for their guidance and support for the fluid aspect of the project, especially for STAR-CCM+.

Finally, I would like to thank **Dr. Erik Van WIJINGAARDEN** from MARIN, Netherlands and **Dr. Tamunoiyala S. KOKO** and **Dr. Brian YUEN** from LR Martec, Canada for their support regarding ComPropApp.

REFERENCES

- Delta journalistic platform tu delft. <https://www.nakashima.co.jp/eng/product/cfrp.html>. Accessed: 2020-02-19.
- Nakashima propeller.co., ltd. <https://www.nakashima.co.jp/eng/product/cfrp.html>. Accessed: 2020-02-19.
- P Atkinson. On the choice of method for the calculation of stress in marine propellers. *Trans RINA*, 110:447–463, 1968.
- JA Bailie, RP Ley, and A Pasricha. A summary and review of composite laminate design guidelines. *National Aeronautics and Space Administration, Final*, (22), 1997.
- Friedrich-Karl Benra, Hans Josef Dohmen, Ji Pei, Sebastian Schuster, and Bo Wan. A comparison of one-way and two-way coupling methods for numerical analysis of fluid-structure interactions. *Journal of applied mathematics*, 2011, 2011.
- Volker Bertram. *Practical ship hydrodynamics*. Elsevier, 2011.
- Amarpreet S Bir, Hsin Piao Chen, and Hsun Hu Chen. *Optimum stacking sequence design of composite sandwich panel using genetic algorithms*, volume 585. Trans Tech Publ, 2012.
- Joseph Boussinesq. *Essai sur la théorie des eaux courantes*. Impr. nationale, 1877.
- John Carlton. *Marine propellers and propulsion*. Butterworth-Heinemann, 2018.
- Jacob Willem Cohen. On stress calculations in helicoidal shells and propeller blades. 1955.
- Derek Hull. Engineering with fibre-polymer laminates: By peter powell. chapman & hall, london, 1994 (441 pp.+ xvii). isbn 0 412 496100 (hb). price:£ 26.99, 1994.
- ML Pavan Kishore and RK Behera. Base line study for determination of effect of stacking sequence on vibration characteristics of composite propeller blade. In *International Conference on Water Resources, Coastal and Ocean, ENGINEERING (ICWRCOE 2015)*, Science Direct, Aquatic Procedia, volume 4, pages 458–465, 2015.

- Alexis Lasseigne. *Optimization of composite structures of 'e variable thickness. Application 'a the CROR blade*. PhD thesis, 2016.
- Hyongsuk Lee, Min-Churl Song, Jung-Chun Suh, and Bong-Jun Chang. Hydro-elastic analysis of marine propellers based on a bem-fem coupled fsi algorithm. *International journal of naval architecture and ocean engineering*, 6(3):562–577, 2014.
- H J Lin, JJ Lin, and Tze-Jer Chuang. Strength evaluation of a composite marine propeller blade. *Journal of reinforced plastics and composites*, 24(17):1791–1807, 2005.
- HJ Lin, WM Lai, and YM Kuo. Effects of stacking sequence on nonlinear hydroelastic behavior of composite propeller blade. *Journal of Mechanics*, 26(3):293–298, 2010.
- Pieter Maljaars, Nicola Grasso, Mirek Kaminski, and Wim Lafeber. Validation of a steady bem-fem coupled simulation with experiments on flexible small scale propellers. In *Proceedings of the Fifth International Symposium on Marine Propulsors, Espoo, Finland*, pages 12–15, 2017a.
- Pieter Maljaars, Laurette Bronswijk, Jaap Windt, Nicola Grasso, and Mirek Kaminski. Experimental validation of fluid–structure interaction computations of flexible composite propellers in open water conditions using bem-fem and rans-fem methods. *Journal of Marine Science and Engineering*, 6(2):51, 2018.
- PJ Maljaars, ML Kaminski, and JH Den Besten. Finite element modelling and model updating of small scale composite propellers. *Composite Structures*, 176:154–163, 2017b.
- MR Motley, Z Liu, and YL Young. Utilizing fluid–structure interactions to improve energy efficiency of composite marine propellers in spatially varying wake. *Composite Structures*, 90(3):304–313, 2009.
- ABHIJIT Mukherjee and B Varughese. Design guidelines for ply drop-off in laminated composite structures. *Composites Part B: Engineering*, 32(2):153–164, 2001.
- Njål Haagensli Munthe-Kaas. Estimating the design parameters of a highly skewed ship propeller by automated 3d-scanning. Master’s thesis, NTNU, 2018.

- S. Paboeuf, B. Collier, and F. and Vialle L. A Berthelot, P. and Le Lay. Composite blade propeller: A design assessment approach. In *4th International Conference on Mechanics of Composites, Madrid, Spain, . mechcomp2018madrid*, 2018.
- Bu-Geun Paik, Gun-Do Kim, Kyung-Youl Kim, Han-Shin Seol, Beom-Soo Hyun, Sang-Gab Lee, and Young-Rae Jung. Investigation on the performance characteristics of the flexible propellers. *Ocean engineering*, 73:139–148, 2013.
- Jean-François Sigrist. *Fluid-structure interaction: an introduction to finite element coupling*. John Wiley & Sons, 2015.
- Mario Alberto Storti, Norberto Marcelo Nigro, Rodrigo Rafael Paz, Lisandro Daniel Dalcín, Gustavo Ríos Rodríguez, and Ezequiel Lopez. Fluid-structure interaction with a staged algorithm. aerospace applications. *CIMEC Document Repository*, 2006.
- D Harsha Vardhan, B Chandra Mohan Reddy, et al. A review on materials used for marine propellers. *Materials Today: Proceedings*, 18:4482–4490, 2019.
- Bureau Veritas. Rule note nr 546 dt r00 e: Hull in composite materials and ply-wood. *Material Approval, Design Principles, Construction and Survey*, 2018.
- F. M. White. *Fluid Mechanics*. McGraw Hill Higher Education, 2006.
- Erik van Wijngaarden. *COMPROPAPP USER’S GUIDE*. MARIN, 2020.
- David C Wilcox et al. *Turbulence modeling for CFD*, volume 2. DCW industries La Canada, CA, 1998.
- Toshio Yamatogi, Hideaki Murayama, Kiyoshi Uzawa, Kazuro Kageyama, and Naoko Watanabe. Study on cavitation erosion of composite materials for marine propeller. In *Seventeenth International Conference on Composite Materials (ICCM17), Edinburgh, UK, July*, pages 27–31, 2009.
- Yin Lu Young, Michael R Motley, Ramona Barber, Eun Jung Chae, and Nitin Garg. Adaptive composite marine propulsors and turbines: progress and challenges. *Applied Mechanics Reviews*, 68(6), 2016.

APPENDIX 1

BENCHMARK STUDY FOR THE COMPARISON OF THE HEXAHEDRAL AND TETRAHEDRAL MESH

In the isotropic blade case, the FSI analysis performed by ComPropApp used hexahedral mesh while the FSI analysis performed by STAR-CCM+ used tetrahedral mesh. Therefore, it was important to carry a benchmark study to compare the difference of the results due to mesh type.

Two isotropic blade models are created; one with hexahedral mesh and the other with tetrahedral mesh. The mesh size is selected after mesh convergence study, hence, the results are independent of the mesh size. The displacement and Von Mises stresses are compared for the two models. The results obtained for both cases are shown in the Fig.46.

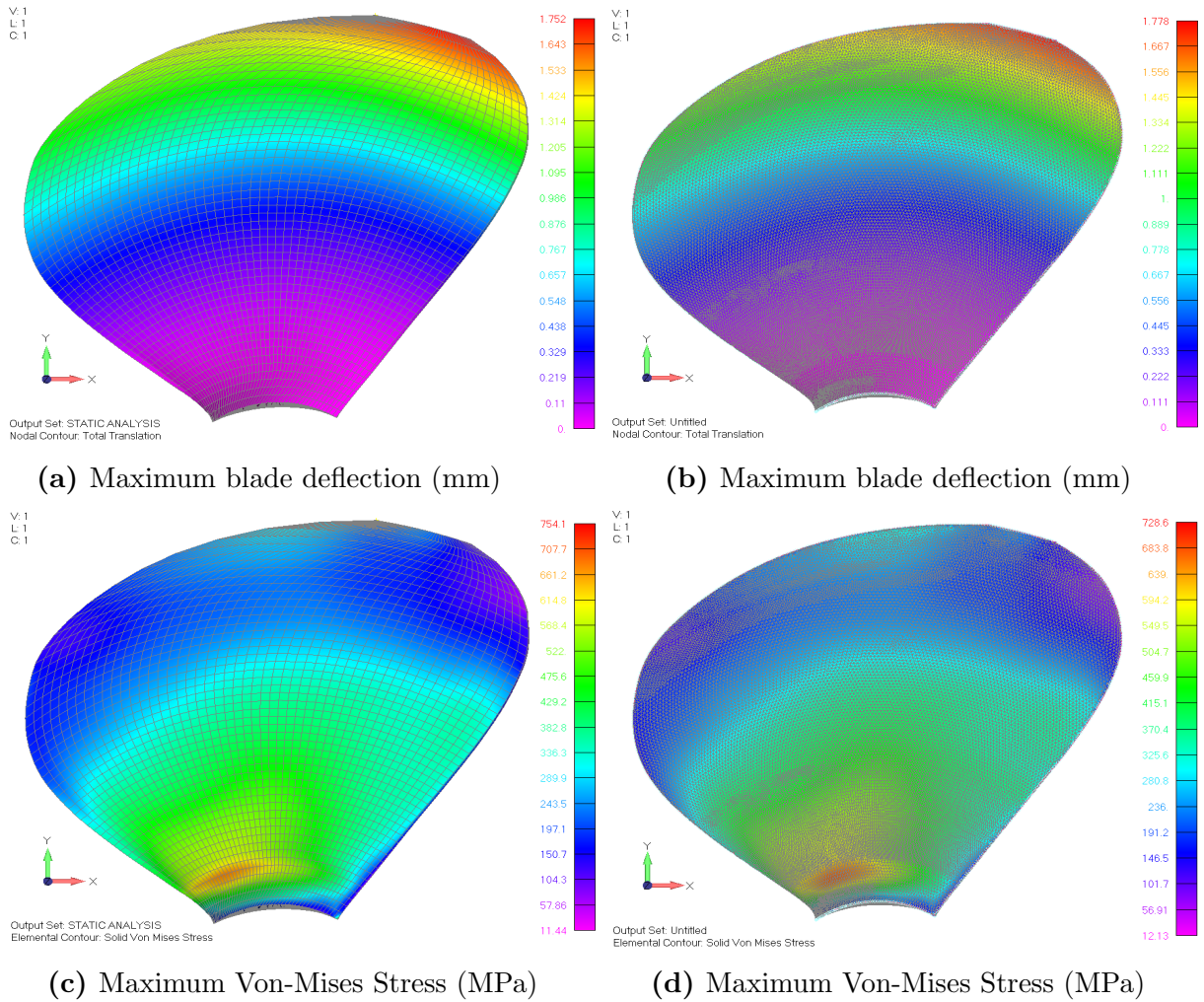


Figure 46: Results obtained in benchmark study

The results obtained are tabulated and compared in the Table.17

Table 17: Comparison of Hexahedral mesh and Tetrahedral mesh

	Hexahedral	Tetrahedral	Relative difference
Max. Deflection (mm)	1.75	1.78	-1.46%
Von-Mises stress (MPa)	754.10	728.60	3.50%

It is noticed that the relative difference for the displacement and stress are ranging from 1.5% to 3.5%. The hexahedral mesh resulted in less displacement and more stresses, same trend is observed by the comparison of the FSI analysis.